A Section 508–conformant HTML version of this article is available at https://doi.org/10.1289/EHP12413.

Xenobiotic Exposure and Migraine-Associated Signaling: A Multimethod Experimental Study Exploring Cellular Assays in Combination with *Ex Vivo* and *In Vivo* Mouse Models

Rikke H. Rasmussen,[1] Sarah L. Christensen,[1] Kirstine Calloe,[2] Brian Skriver Nielsen,[3] Anders Rehfeld,[3] Thomas E. Taylor-Clark,[4] Kristian A. Haanes,[5,6] Olivier Taboureau,[7] Karine Audouze,[8] Dan A. Klaerke,[2] Jes Olesen,[1] and David M. Kristensen[3,9,10]

[1]Department of Neurology, Danish Headache Center, Copenhagen University Hospital – Rigshospitalet, Glostrup, Denmark
[2]Department of Veterinary and Animal Sciences, Faculty of Health and Medical Sciences, University of Copenhagen, Frederiksberg C, Denmark
[3]Department of Growth and Reproduction, Copenhagen University Hospital – Rigshospitalet, Copenhagen, Denmark
[4]Department of Molecular Pharmacology and Physiology, Morsani College of Medicine, University of South Florida, Tampa, USA
[5]Department of Clinical Experimental Research, Rigshospitalet Glostrup, Glostrup, Denmark
[6]Department of Biology, Section of Cell Biology and Physiology, University of Copenhagen, Denmark
[7]Unité de Biologie Fonctionnelle, Université Paris Cité, Centre national de la recherche scientifique (CNRS, French National Centre for Scientific Research), Institut national de la santé et de la recherche médicale (Inserm, National Institute of Health & Medical Research), Paris, France
[8]Université Paris Cité, T3S, Inserm U1124, Paris, France
[9]Institut de recherche en santé, environnement et travail (Irset) – UMR_S 1085, Université de Rennes, Inserm, École des hautes études en santé publique (EHESP), Rennes, France
[10]Department of Science and Environment, Roskilde University, Roskilde, Denmark

Background: Mechanisms for how environmental chemicals might influence pain has received little attention. Epidemiological studies suggest that environmental factors such as pollutants might play a role in migraine prevalence. Potential targets for pollutants are the transient receptor potential (TRP) channels ankyrin 1 (TRPA1) and vanilloid 1 (TRPV1), which on activation release pain-inducing neuropeptide calcitonin gene-related peptide (CGRP).

Objective: In this study, we aimed to examine the hypothesis that environmental pollutants via TRP channel signaling and subsequent CGRP release trigger migraine signaling and pain.

Methods: A calcium imaging–based screen of environmental chemicals was used to investigate activation of migraine pain–associated TRP channels TRPA1 and TRPV1. Based on this screen, whole-cell patch clamp and *in silico* docking were performed for the pesticide pentachlorophenol (PCP) as proof of concept. Subsequently, PCP-mediated release of CGRP and vasodilatory responses of cerebral arteries were investigated. Finally, we tested whether PCP could induce a TRPA1-dependent induction of cutaneous hypersensitivity *in vivo* in mice as a model of migraine-like pain.

Results: A total of 16 out of the 52 screened environmental chemicals activated TRPA1 at 10 or 100 μM. None of the investigated compounds activated TRPV1. Using PCP as a model of chemical interaction with TRPA1, *in silico* molecular modeling suggested that PCP is stabilized in a lipid-binding pocket of TRPA1 in comparison with TRPV1. *In vitro*, *ex vivo*, and *in vivo* experiments showed that PCP induced calcium influx in neurons and resulted in a TRPA1-dependent CGRP release from the brainstem and dilation of cerebral arteries. In a mouse model of migraine-like pain, PCP induced a TRPA1-dependent increased pain response ($N_{total} = 144$).

Discussion: Here we show that multiple environmental pollutants interact with the TRPA1-CGRP migraine pain pathway. The data provide valuable insights into how environmental chemicals can interact with neurobiology and provide a potential mechanism for putative increases in migraine prevalence over the last decades. https://doi.org/10.1289/EHP12413

Introduction

In 2016, the World Health Organization (WHO) found migraine to be the second largest cause of disability worldwide only exceeded by low back pain.[1] It is debated whether the prevalence of migraine is rising or remaining stable. Several studies have reported that the prevalence of migraine is increasing in both adults and children,[2–4] with rates that exclude genetics as the driving cause.[4] Other studies contradict these data,[5,6] whereas a systematic review and meta-analysis from 2017 including 302 studies found a pattern of rising prevalence.[7] If the prevalence is increasing, the underlying reasons are likely a complex combination of increased public awareness, better medical diagnostics, and changes in the environment, with chemicals previously suggested to play a role.[8–11]

The burden of exposure to environmental chemicals that are foreign to the human body (also called xenobiotics) has increased during the past several decades.[12] These pollutants include chemicals such as parabens, phthalates, ultraviolet filters, pesticides, perfluoroalkylated substances, and pharmaceuticals, among others. Although the effect of such chemicals on the developing brain has caused much concern—leading to the TENDR consensus statement calling for reduction of exposures to toxic chemicals that can contribute to disruption of neurodevelopment[13]—the potential effects on the adult brain has received less attention.

The scent from the California bay laurel tree (*Umbellularia californica*), also known as "the headache tree," is known to trigger headache attacks, as well as sneezing, sinus irritation, and unconsciousness.[14,15] Researchers found that the naturally occurring chemical, umbellulone, which is emitted from the tree, can activate pain pathways associated with migraine.[16] Umbellulone activates the transient receptor potential ankyrin 1 (TRPA1) channel, with subsequent release of neuropeptide calcitonin gene-related peptide (CGRP) *in vitro*.[16] CGRP release is a well-characterized mechanism underlying migraine attacks, and several migraine therapeutics target CGRP or its receptor.[17,18] Besides TRPA1, the transient receptor potential vanilloid 1 (TRPV1) ion channel

Address correspondence to David M. Kristensen, Department of Growth and Reproduction, Copenhagen University Hospital – Rigshospitalet, Copenhagen, Denmark. Email: david.moebjerg.boslev.kristensen@regionh.dk

Supplemental Material is available online (https://doi.org/10.1289/EHP12413).
All authors report no competing interests.
Received 9 November 2022; Revised 13 September 2023; Accepted 25 September 2023; Published 1 November 2023.

Note to readers with disabilities: *EHP* strives to ensure that all journal content is accessible to all readers. However, some figures and Supplemental Material published in *EHP* articles may not conform to 508 standards due to the complexity of the information being presented. If you need assistance accessing journal content, please contact ehpsubmissions@niehs.nih.gov. Our staff will work with you to assess and meet your accessibility needs within 3 working days.

is also suggested to be involved in migraine signaling through release of CGRP. TRPA1 and TRPV1 are coexpressed in trigeminal sensory neurons together with CGRP that on its release causes vasodilation, sensitization, and ultimately an increase in the perception of pain.[19,20]

We tested whether abundant environmental chemicals could, similarly to umbellulone, activate the TRPA1 and TRPV1 pain pathways using a combination of *in vitro*, *in silico*, *ex vivo*, and *in vivo* techniques. We hypothesized that the increased exposure to xenobiotics might play a role in migraine prevalence.

Methods

Cells and Cultivation

Transfected cell lines. HEK293 cells stably transfected with either the human TRPA1 channel (hTRPA1-HEK) human TRPV1 channel (hTRPV1-HEK) or control plasmid (control cells) were used in this study. hTRPA1-HEK and hTRPV1-HEK cells were provided by coauthor T.T. Control cells were generated from in-house stocks of HEK-293 cells originally purchased from ATCC (Cat. no. CLR-1573) using FuGENE HD Transfection Reagent (Cat. no. E2311; Promega) and control plasmid [originally purchased from Clontech (Takara Bio) but is now found at NovoPro Bioscience Inc. (Cat. no. V012021] with neomycin/G418 as selection marker, similar to the plasmids used for generation of hTRPA1-HEK and hTRV1-HEK cells. Therefore, all three cell lines were continuously kept under antibiotic selection to ensure plasmid expression. Transfection was performed following the manual provided with the FuGENE HD Transfection Reagent (Cat. no. E2311; Promega). In short, cells were seeded (300,000 cells per well) in a 6-well culture plate (Cat. no. 140675; Thermo Fisher Scientific) on day 1. After reaching 80% confluency (day 2), cells were transfected with a FuGENE HD:DNA ratio of 3:1. On day 3, the selection antibiotic G418 (Geneticin, Cat. no. 10131035; Gibco, Thermo Fisher Scientific) (600 μg/mL) was introduced and continuously supplied to the media to ensure plasmid expression for 3 wk. All three cell lines were cultured in Dulbecco's Modified Eagle's Medium (DMEM; Cat. no. 41965062; Gibco, Thermo Fisher Scientific) supplemented with 10% fetal bovine serum (Cat. no. F9665; Sigma-Aldrich), 1% GlutaMAX Cat. no. 35050061; Gibco, Thermo Fisher Scientific), 1% penicillin-streptomycin (10,000 U/mL) (Cat. no. 15140122; Gibco, Thermo Fisher Scientific), and 500 μg/mL G418 (Geneticin) (Cat. no. 10131035; Gibco, Thermo Fisher Scientific). The cells were maintained in a humidified incubator (37°C, 5% CO_2). The cells lines were initially and continuously tested for selective responsiveness to the TRPA1 agonist supercinnamaldehyde (SCA) and the TRPV1 agonist capsaicin to confirm expression using calcium imaging as described in the "Methods" section titled "Calcium Imaging." Results can be seen in Figure 1A.

Primary cell culture. Trigeminal neurons were isolated following a modified version of the method described in Materazzi et al.[21] A total of eight C57BL/6JbomTac pups (bred in house and sex not determined) were euthanized at postnatal days 5–7. The trigeminal ganglia (TG) were bilaterally excised, washed in DPBS (Cat. no. 14190250; Gibco, Thermo Fisher Scientific) and digested in 0.25% collagenase type IV (Cat. no. C5138; Sigma-Aldrich) in DMEM/F12 (Cat. no. 31331093; Gibco, Thermo Fisher Scientific) for 60 min at 37°C following mechanical digestion by pipetting. The supernatant was centrifuged at 100 × *g* for 3 min, and the pellet was resuspended in DMEM/F12 with 5% fetal bovine serum (Cat. no. F9665; Sigma-Aldrich), 1% penicillin-streptomycin (10,000 U/mL) (Cat. no. 15140122; Gibco, Thermo Fisher Scientific), 100 ng/mL NGF (Cat. no. SRP4304; Sigma-Aldrich), 2 μM cytosine-b-arabinofuranoside (Cat. no. C6645; Sigma-Aldrich) and 2.5 μg/mL Amphotericin B (Cat. no. 15290018; Gibco, Thermo Fisher Scientific). Viability of the cells was determined before plating using a Nucleocounter NC-200 (Chemometec) and Via1-Casettes (Cat. no. 941-0012; Chemometec). Viability ranged from 80% to 90%. Cells were plated in 35 mm (120,000 cells per dish) 0.01 mg/mL Poly-D-Lysine (Cat. no. P6407; Sigma-Aldrich)–coated dishes (Cat. no. 627160; Greiner Bio-One) and cultured 1–2 d in a humidified incubator (37°C, 5% CO_2) before patch clamp experiments.

Cytotoxicity

Measurement of cytotoxicity was performed in accordance with the manual provided with Invitrogen alamarBlue HS Cell Viability Reagent (Cat. no. A05101; Thermo Fisher Scientific). One day prior to measuring, hTPRA1-HEK cells were seeded at a density of 25,000 cells/well (90 μL) in Poly-D-Lysine–coated 96-well plates (Cat. no. 734-0317; VWR International). Cells were treated with PCP in increasing concentrations (1 μM, 10 μM, and 100 μM) for 1 h. AlamarBlue (10 μL) was added to the cells and incubated for 1 h. Viability was measured with absorbance at 570 nm, with 600 nm as reference using a plate photometer (Infinite M200; Tecan) with software [SW Magellan (version 6.3)]. Data are normalized to the vehicle (0.1% DMSO). Positive control was 10 μM ionomycin.

Calcium Imaging

Calcium imaging was performed in accordance with the manual provided with Invitrogen Fluo-4 Direct Calcium Assay Kit (Cat. no. F10471; Thermo Fisher Scientific). One day prior to calcium imaging, cells were seeded at a density of 25,000 cells/well (50 μL) in Corning BioCoat Poly D-Lysine–coated 96-well plates (Cat. no. 734-0317; VWR International). Cells were kept in an incubator for 1 day (37°C, 5% CO_2) before testing and reached a confluency of ∼ 80%–90%. Using the Invitrogen Fluo-4 Direct Calcium Assay Kit (Cat. no. F10471; Thermo Fisher Scientific), cells were loaded with 2x Fluo-4 Direct calcium reagent loading solution (5 mM probenecid) following incubation (37°C, 5% CO_2) for 90–120 min. Blank wells were loaded with Fluo-4 Direct calcium assay buffer. Changes in intracellular calcium concentration were measured using the multifunctional microplate reader NOVOstar (BMG Labtech). Instrument settings were excitation at 494 nm and emission at 516 nm. Fluorescence was monitored every 0.3 s for 70.6 s. The baseline fluorescence of each well was measured for 1.2 s prior to injection of test chemicals or controls. The baseline fluorescence was used to align the fluorescence within each well. Every plate included blank wells (–dye, injection: buffer), negative control (+dye, injection: buffer+vehicle), two positive controls [+dye, injection: 10 μM capsaicin (Cat. no. M2028; Sigma-Aldrich) or 10 μM SCA (Cat. no. S3322; Sigma-Aldrich)] and [+dye, injection: 10 μM ionomycin (Cat. no. I24222; Invitrogen, Sigma-Aldrich)] and wells used for testing different chemicals [+dye, injection: test chemical (10–100 μM)]. The ionophore, ionomycin, was used as a positive control to measure the maximal Ca2+ uptake in the cells.[22] Blank wells served to measure the background fluorescence. The mean background fluorescence was subtracted from all other wells prior to any data handling. The mean baseline fluorescence for each individual well was subtracted from the fluorescence measured at all time points. Relative fluorescence unit (RFU) is the fluorescence measured after subtracting background fluorescence and well-specific baseline fluorescence. Effect sizes were calculated as percentage of ionomycin to allow comparison between cell lines:

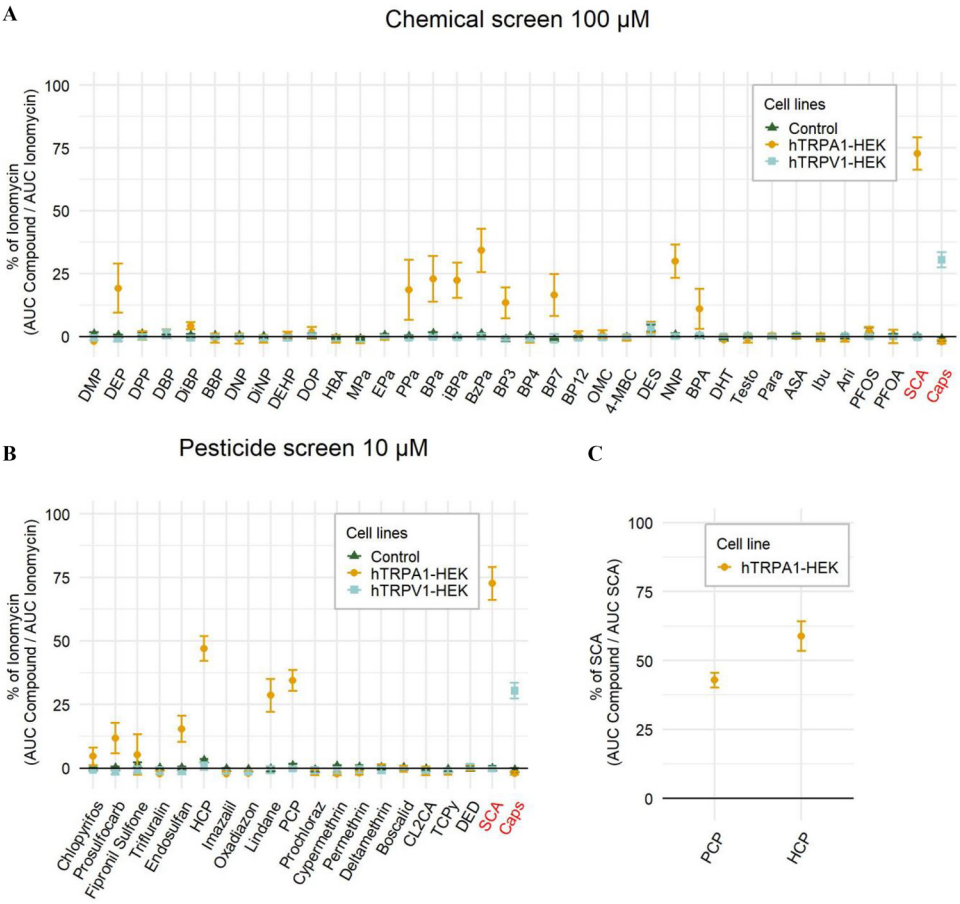

Figure 1. Calcium imaging of environmental chemicals using hTRPA1-HEK and hTRPV1-HEK cell lines. Calcium imaging was performed using fluo-4 following acute exposure to 52 chemicals. Cells were seeded at a density of 25,000 cells/well in a 96-well plate 1 day prior to imaging and recordings were performed every 0.3 s for 70.6 s using a NOVOstar microplate reader. (A) Summary of calcium imaging data of chemical screen (100 µM). Numeric data are found in Table S1. (B) Summary of calcium imaging data of pesticide screen (10 µM). Numeric data are found in Table S2. For (A) and (B) calcium imaging was performed using hTRPA1-HEK (yellow circle), hTRPV1-HEK (blue square), and control cells (green triangle). Responses were normalized to the ionomycin response (10 µM). (C) Calcium imaging response normalized to supercinnamaldehyde (SCA) response for PCP and HCP in hTRPA1-HEK. Numeric data are found in Table S3. (A–C) The screen was repeated twice with 3–6 technical replicates within each plate. The data are presented as a weighted mean from repeated experiments, and whiskers represent the combined SD from repeated screens. TRPA1 agonist supercinnamaldehyde (SCA) and TRPV1 agonist capsaicin (caps) were tested in all three cell lines. For abbreviations of chemicals see Tables 1 and 2. Note: HCP, hexachlorophene; PCP, pentachlorophenol.

$$percentage\ of\ ionomycin = \frac{AUC(test\ compound) - AUC(vehicle)}{AUC(test\ ionomycin) - AUC(vehicle)}. \quad (1)$$

For pentachlorophenol and hexachlorophene, effect sizes were calculated as percentage of SCA to show the response relative to maximal TRPA1 activation:

$$percentage\ of\ SCA = \frac{AUC\,(test\ compound) - AUC\,(vehicle)}{AUC\,(test\ SCA) - AUC\,(vehicle)}. \quad (2)$$

The screen was repeated twice with 3–6 technical replicates ($n = 3$–6) within one plate. Data are presented as weighted means from repeated screens, and the standard deviation (SD) is calculated as a combined SD from repeated screens ($n = 2$).

Electrophysiology

hTRPA1-HEK ($n = 3$) and control cells ($n = 4$) were used for whole-cell voltage clamp recordings using a MultiClamp 700B amplifier and MultiClamp Commander. pCLAMP 10.7 software (Molecular Devices) was used for acquisition and analysis. Glass capillary microelectrodes were pulled to a resistance of 1.5–2.5 MΩ and then filled with the pipette solution: (in mM): 140 CsCl, 5 EGTA, 10 HEPES, 0.2 Na_2-GTP, and 2 Na_2-ATP with pH adjusted to 7.2 with CsOH. The extracellular solution contained (in mM): 140 NaCl, 5 KCl, 1 $MgCl_2$, 2 $CaCl_2$, and 10 HEPES with pH adjusted to 7.4 with NaOH as described in Yoo et al.[23] Currents were activated using a voltage ramp protocol from −100 to +100 mV over 325 ms from a holding potential of −60 mV performed at 36°C. Whole-cell recordings of primary trigeminal neurons ($n = 10$) followed a method modified from Benemei et al.[24] Glass capillary microelectrodes (1.5–2.5 MΩ) were filled with the pipette solution described above. The extracellular solution contained (in mM): 147 NaCl, 4 KCl, 1 $MgCl_2$, 5 $CaCl_2O$, and 10 HEPES with pH adjusted to 7.4 with NaOH. Current measurements were performed at a constant potential of −60 mV at room temperature 22°C. Because of the inactivation of TRPA1 after PCP exposure, cells were replaced for each experiment. Five out of 15 cells did not respond and were not included in the data set. This was expected because TRPA1 expression and activation is seen in a subset of TG neurons.[16,25] Data are graphically presented as means and standard error of the means (SEM).

Molecular Modeling

Several cryo-EM structures of hTRPA1 are available on the PDB databank (as of December 2021; https://www.rcsb.org/). The 3D structure 6×2j.pdb corresponding to the human TRPA1 complexed with the noncovalent agonist GNE551 (5-amino-1-1[(4-bromo-2-fluorophenyl)methyl]-*N*-(2,5-dimethoxyphenyl)-1H-1,2,3-triazole-4-carboxamide) was used in this study[26] to assess the mechanism of binding of acrolein (a known hTRPA1 activator)[9–11] and PCP (a suggested hTRPA1 activator from our experimental study). Regarding hTRPV1, the crystal structure of the human channel is not yet elucidated, but cryo-EM structures of the full length of squirrel TRPV1 complexed with capsaicin (a well-known agonist of TRPV1)[27,28] are available and can be used to develop a structural model of hTRPV1. In our case, we exploited the cryo-EM structure 7lpb.pdb[29] and developed a hTRPV1 model using the SWISS Model server (https://swissmodel.expasy.org/). Both structures (hTRPA1 and hTRPV1) were protonated using the licensed software MOE (version 2020.09; http://www.chemcomp.com). A pocket surrounding the GNE551 ligand in TRPA1 and a lipid pocket in TRPV1 were considered for the docking of PCP and acrolein. The docking method implemented in MOE was used. Only the ligands were flexible in the used model, meaning that the entire inner pockets of TRPA1 and TRPV1 were kept rigid. The docking module in MOE uses an affinity scoring function to assess candidate poses. The number of poses was set to 10, and only the poses with the highest affinity scores were analyzed.

Experimental Animals

Experiments were performed under license number 2017-15-0201-01358 from the Danish Animal Experiments Inspectorate and in accordance with the European Community guide for the care and use of animals (2010/63/UE). A total of 136 adult mice and 8 pups were used to complete the study. The eight wild type pups were used for primary cell culture and bred in house under license number 2021-15-0206-00015. A total of 31 male wild type C57BL/6JbomTac mice (Taconic Biosciences) and 25 male C57BL/6J-*Trpa1*$^{-/-}$ mice (*Trpa1*$^{-/-}$) [Trpa1tm1/Dpc[30] in house breeding (license number 2018-15-0202-00162) derived from breeders donated by Peter Reeh, Friedrich-Alexander-University of Erlangen–Nürnberg] 8–16 wk of age were used for CGRP release and vasoactivity studies. A total of 24 male and 24 female wild type C57BL/6JbomTac mice (Taconic Biosciences) (9–13 wk of age) and 16 male and 16 female *Trpa1*$^{-/-}$ mice (in-house breeding) (11–16 wk of age) were used for von Frey testing. Mice weighed between 17 and 33 g. Mice were group-housed under a 12-h light/dark cycle in a climate-controlled room (24°C, 55% humidity) with free access to food and water and with several shelters and two types of nesting material as enrichment. All behavioral experiments were carried out in low-light conditions (20–30 lux). Experiments were planned and carried out to comply with ARRIVE guidelines.

Ex Vivo *CGRP Release*

The CGRP release experiments were carried out as previously described.[31] Wild type ($n = 27$) and *Trpa1*$^{-/-}$ mice ($n = 25$) (9–16 wk of age) were anesthetized using 70% CO_2 in 30% O_2, followed by decapitation. The brain stem including the trigeminal nucleus caudalis (TNC) was isolated by removing the dorsal part of the cervical vertebras as well as removing the posterior part of the skull covering the cerebellum. The cerebellum was removed to expose the brain stem. The TNC-containing part of the brain stem was then separated from the brain and immersed into synthetic interstitial fluid (SIF) buffer. The brain stem was washed in SIF buffer for 30 min, replacing SIF every 5 min. The brain stem was then transferred to Eppendorf lids containing 250 μL SIF and placed in an incubator (37°C). SIF was replaced every 5 min for 20 min. The basal CGRP release was determined by sampling 200 μL after 10 min incubation in 250 μL SIF. SCA or PCP was tested in the range of 1 μM–100 μM. Starting with the lowest concentration, 250 μL SCA or PCP was added to the tissue, and a sample of 200 μL was collected after 10 min incubation (37°C). At the end of each experiment, the tissue was incubated with 10 μM capsaicin as a positive control to assess the ability of the tissue to release CGRP. All samples were immediately mixed with 50 μL enzyme immunoassay (EIA) buffer provided with the commercially available ELISA kit (Cat. no. A05482; Bertin Bioreagent) and stored at −20°C. Composition of SIF: 108 mM NaCl, 3.48 mM KCl, 3.50 mM $MgSO_4$, 26 mM $NaHCO_3$, 11.70 mM NaH_2PO_4, 1.50 mM $CaCl_2$, 9.60 mM Na-gluconate, 5.50 mM glucose, and 7.60 mM sucrose with pH adjusted to 7.4 and stabilized by carbogen gassing. CGRP levels were then measured with a commercially available ELISA kit (Cat. no. A05482; Bertin Bioreagent) using the standard protocol supplied by the manufacturer. Samples were diluted in SIF and EIA buffer to fit the range of the standard curve. The optical density was measured at 410 nm using a plate photometer (Infinite M200; Tecan) with software (SW Magellan version 6.3). Values were normalized to the basal CGRP release to account for differences in size of tissue pieces. The data are presented graphically as means and SEM.

Ex Vivo *Vasoactivity*

Male mice [wild type ($n = 4$) or *Trpa1*$^{-/-}$ ($n = 4$)] at the age of 8–10 wk were anesthetized using 70% CO_2 in 30% O_2, followed by decapitation. Measurement of vasoactivity was performed following a procedure modified from Mulvany and Halpern.[32,33] The brain was carefully released from the skull and immersed in cold oxygenated calcium-free Krebs buffer (Ca^{2+}-free Krebs). The basilar artery was gently dissected and divided into two segments with an equal length of ∼1 mm. Once the basilar artery (BA) segments were mounted on 25-μm diameter wires, in a Mulvany-Halpern wire myograph (Danish Myo Technology), the buffer was changed to Na^+Krebs (with calcium) and heated to 37°C. Following 15 min of equilibration, the vessels were stretched to reach a pretension of ∼ 2 mN/mm. Initially, K^+Krebs (60 mM K^+) was added to examine the contractile potential of the BA. Subsequently, half of the segments were treated with 1 μM CGRP antibody (CGRPab, fremanezumab; Teva Pharmaceutical Industries Ltd.), an antibody directed against human CGRP. After 30 min of stabilization, precontraction of all segments was achieved by addition of 0.3 μM U46619 (Cat. no. 1932; Tocris)—a synthetic PGH_2 analog. When a stable precontraction was achieved, a cumulative concentration–response curve to PCP (0.1–30 μM) was performed. At the end of each experiment, the vascular smooth muscle cell contractile function/viability was tested by adding K^+Krebs again. Na^+Krebs is composed of 119 mM NaCl, 4.6 mM KCl, 1.5 mM $CaCl_2$, 1.2 mM $MgCl_2$, 1.2 mM NaH_2PO_4, 15 $NaHCO_3$, 5.5 mM glucose, and 0.03 mM EDTA; pH 7.4. K^+Krebs is similar to Na^+Krebs, except that 55.4 mM NaCl is exchanged for KCl on equimolar, making it 60 mM K^+. Myograph responses were collected in LabChart (ADInstruments). Percentage of precontraction was calculated as:

$$\text{percentage of precontraction} = \left(100 \times \frac{x - \textit{max relaxation potential}}{100\%\ \textit{precontraction} - \textit{max relaxation potential}}\right), \quad (3)$$

where x is the tension of the blood vessel after stimulation. For individual blood vessels, 100% precontraction and resting tension are constants.

In Vivo Mouse Model

To investigate the possible activation of nociceptive pathways *in vivo*,[34–37] we evaluated sensitivity to tactile stimulation with von Frey filaments as a surrogate marker of pain following PCP treatment (15 mg/kg p.o. dissolved in 0.5% carboxymethylcellulose, CMC in water given by oral gavage [feeding needles: Cat. no. 5202; AgnTho's AB)]. First, 16 male and 16 female wild type mice received either PCP ($n = 16$) or vehicle ($n = 16$) daily for a total of 9 d to test the acute and potential cumulative effect. Mice were subject to von Frey test 2 and 4 h after the first administration (acute sensitivity) and on selected days (5, 6, 8, and 10) prior to administration of PCP (basal/chronic sensitivity) (see Figure 5A,B). In a second experiment (see Figure 5D), 16 male and 16 female *Trpa1*$^{-/-}$ mice received a single treatment of either PCP ($n = 16$) or vehicle ($n = 16$), and 8 male and 8 female wild type mice received PCP to test the acute effect of PCP and TRPA1 dependency. For the von Frey test, mice were placed in individual clear plexiglass chambers on a mesh floor (IITC Life Science). Separate chambers were used for male and female mice. Mice were acclimatized in test champers for 30–45 min prior to testing. Chambers were cleaned with soap wipes after each test. Von Frey monofilaments [0.008 g, 0.02 g, 0.04 g, 0.07 g, 0.16 g, 0.4 g, 0.6 g, 1 g, 2 g (Cat. no. 37450-275; Ugo Basile)] were applied to the plantar surface of the left hind paw (between foot pads) according to the up-down paradigm.[38,39] In one smooth motion, filaments were applied perpendicular to the skin and bent to maximum force for 2–3 s or until withdrawal. The 0.16 g filament was applied first, and on positive withdrawal response (rapid lifting or licking of the paw), the lighter filament was applied next. On no response, the heavier filament was applied. Four filaments were applied after the first breaking point (response–no response or no response–response). Calculation of 50% withdrawal thresholds was done using the free online calculator at https://bioapps.shinyapps.io/von_frey_app/, with application of exact interfilament steps and target force as input variables.[40] Calculated values above or below the filament range were manually assigned 2 g and 0.008 g, respectively. All testing was performed between 0800 (8 A.M.) and 1600 (4 P.M.) by an experimenter blinded to treatment groups. To prevent contamination between treatment groups, home cages were restricted to one treatment, and allocation of treatment was randomized but counterbalanced in relation to sex and baseline sensitivity to avoid confounding by these factors. Group sizes of 16 were based on in-house previous work with chemical induction of mechanical hypersensitivity, where group sizes of 10–12 provided adequate power to detect differences between treatment groups when effect size was intermediate.[35,37,41] Here, we expected a smaller effect size and increased the number of mice per group. No animals were excluded from the experiment. Fifty percent withdrawal thresholds were square root–transformed for improved Gaussian distribution,[42,43] and data are presented as means and SEM.

Motor Function

To demonstrate that the von Frey test was not biased by impaired motor function or sedation as a potential side effect of PCP, general motor function was assessed using a rotarod (RotaRod Advanced; IITC Life Science Inc.). The mice were tested four times in total—before PCP administration (baseline), 2 h and 4 h after PCP administration, and 10 min after 2 mg/kg midazolam or saline (i.p.) administration as a control. Mice were placed on the rotarod with a start speed of 0 rpm, which increased to 30 rpm with a ramp of 45 s and terminated after 150 s (maximum duration). The time spent on the rotarod was recorded. Following the first von Frey experiment (see Figure 5A–C), 32 wild type mice received either 2 mg/kg midazolam (i.p.) ($n = 16$) or saline ($n = 16$) 10 min prior to rotarod testing on day 10. Following the second von Frey experiment (see Figure 5D,E), 48 mice (wild type $n = 16$ and *Trpa1*$^{-/-}$ $n = 32$) received either 2 mg/kg midazolam (i.p) ($n = 24$) or saline ($n = 24$) 10 min prior to rotarod testing on day 1. Mice were randomly allocated according to sex, previous treatment, and genotype when given midazolam to avoid confounding by these factors. No animals were excluded. Rotarod data are expressed graphically as plots with individual data points and medians. The data are described in text by median and 95% confidence intervals (CIs).

Chemicals

All chemicals, except ibuprofen, tested in the initial "chemical screen 100 μM" were dissolved in 99% ethanol to a stock concentration of 100 mM and stored at −80°C. Ibuprofen was dissolved in 100% dimethylsulfoxide (DMSO) to a stock concentration of 100 mM. Pesticides tested in the "Pesticide screen 10 μM" were dissolved in 100% DMSO to a stock concentration of 10 mM and stored at −20°C. All chemicals were originally purchased from Sigma-Aldrich. Chemicals in the "chemical screen" were screened because they were part of an established chemical library developed by coauthor D.M.K. Pesticides included in the "pesticide screen" were screened because they were originally part of an established pesticide library by coauthor A.R. We chose to test the chemicals in the "chemical screen" at the highest concentration possible (100 μM) and because of the toxic nature of pesticides, we chose to test these at a 10-fold lower concentration (10 μM). The screens were performed sequentially to optimize the workflow because of the difference in concentration. Ionomycin (Cat. no. I24222; Invitrogen, Sigma-Aldrich) was dissolved in 100% DMSO to a stock concentration of 1 mM. PCP (Cat. no. P2604; Sigma-Aldrich) and SCA (Cat. no. S3322; Sigma-Aldrich) used in CGRP release experiments and vasoactivity experiments were dissolved in 100% DMSO to a stock concentration of 100 mM. A list of chemicals tested is available in Tables 1 and 2. All chemicals tested in calcium imaging, CGRP release, or vasoactivity experiments were diluted in aqueous buffer fresh on the day of experiments and kept on ice until used. For whole-cell patch clamp experiments, HC-030031 (H4415; Sigma-Aldrich) was diluted in 100% DMSO to a stock concentration of 100 μM. PCP and HC-030031 were diluted in aqueous buffer on the day of experiments and kept at room temperature until used. For *in vivo* experiments, PCP was dissolved in DMSO and further diluted in 0.5% CMC in water before p.o. administration. Midazolam (1 mg/mL hydrochloride; Hameln Pharma) was dissolved in saline.

Statistical Analyses

For results from patch clamp of HEK cells, a one-way ANOVA followed by Bonferroni's multiple comparisons test was applied. For patch clamp of TG neurons, cells exhibited a varied response, and the data did not follow a normal distribution. Therefore, a Wilcoxon matched-pairs signed rank test was used. In *ex vivo* CGRP release studies, statistical analyses between SCA or PCP and vehicle were performed using multiple unpaired *t*-tests with post hoc Holm-Šidák correction. In *ex vivo* vasoactivity studies, a two-way ANOVA was performed. For von Frey studies, data were square root (SQRT) transformed for improved Gaussian distribution and analyzed by a two-way repeated measures mixed model including Geisser-Greenhouse correction. Subsequently, post hoc comparison between test groups was performed with Dunnett's correction for multiple comparisons when multiple test groups were tested against the vehicle group and Šidák's correction when only two groups were compared. Groups were randomized according to baseline 50% withdrawal thresholds. For motor function studies, the data were analyzed by multiple Mann-Whitney tests with Holm-Šidák post hoc comparison when two groups were compared and by Kruskal-

Table 1. List of chemicals used for chemical screen.

Group	Common name	IUPAC name	Abbreviation	CAS number
Phthalates	Dimethyl phthalate	Dimethyl benzene-1,2-dicarboxylate	DMP	131-11-3
	Diethyl phthalate	Diethyl benzene-1,2-dicarboxylate	DEP	84-66-2
	Di-*n*-pentyl phthalate	Dipentyl benzene-1,2-dicarboxylate	DPP	131-18-0
	Di-*n*-butyl phthalate	Dibutyl benzene-1,2-dicarboxylate	DBP	84-74-2
	Diisobutyl phthalate	Bis(2-methylpropyl) benzene-1,2-dicarboxylate	DiBP	84-69-5
	Benzyl butyl phthalate	Benzyl butyl benzene-1,2-dicarboxylate	BBP	85-68-7
	Di-*n*-nonyl phthalate	Dinonyl benzene-1,2-dicarboxylate	DNP	84-76-4
	Diisononyl phthalate	Bis(7-methyloctyl) benzene-1,2-dicarboxylate	DiNP	68515-48-0
	Di(2-ethylhexyl) phthalate	Bis(2-ethylhexyl) benzene-1,2-dicarboxylate	DEHP	117-81-7
	Di-*n*-octyl phthalate	Dioctyl benzene-1,2-dicarboxylate	DOP	117-84-0
Parabens	4-hydroxybenzoic acid	4-hydroxybenzoic acid	HBA	99-96-7
	Methyl paraben	Methyl 4-hydroxybenzoate	Mpa	99-76-3
	Ethyl paraben	Ethyl 4-hydroxybenzoate	Epa	120-47-8
	Propyl paraben	Propyl 4-hydroxybenzoate	Ppa	94-13-3
	Butyl paraben	Butyl 4-hydroxybenzoate	Bpa	94-26-8
	Iso-butyl paraben	2-methylpropyl 4-hydroxybenzoate	iBPa	4247-02-3
	Benzyl paraben	Benzyl 4-hydroxybenzoate	BzPa	94-18-8
UV filters	Benzophenone 3	(2-hydroxy-4-methoxyphenyl)-phenylmethanone	BP3	131-57-7
	Benzophenone 4	5-benzoyl-4-hydroxy-2-methoxybenzenesulfonic acid	BP4	4065-45-6
	Benzophenone 7	(5-chloro-2-hydroxyphenyl)-phenylmethanone	BP7	85-19-8
	Benzophenone 12	(2-hydroxy-4-octoxyphenyl)-phenylmethanone	BP12	1843-05-6
	Octinoxate	2-ethylhexyl I-3-(4-methoxyphenyl)prop-2-enoate	OMC	5466-77-3
	4-methylbenzylidene camphor	(3*Z*)-1,7,7-trimethyl-3-[(4-methylphenyl)methylidene]bicyclo[2.2.1] heptan-2-one	4-MBC	36861-47-9
Naturally occurring hormones or hormone-like compounds	Diethylstilbestrol	4-[(E)-4-(4-hydroxyphenyl)hex-3-en-3-yl]phenol	DES	56-53-1
	Nonyl phenol	4-nonylphenol	NNP	84852-15-3
	Bisphenol A	4-[2-(4-hydroxyphenyl)propan-2-yl]phenol	BPA	80-05-7
	Dihydrotestosterone	(5*S*,8*R*,9*S*,10*S*,13*S*,14*S*,17*S*)-17-hydroxy-10,13-dimethyl-1,2,4,5,6,7,8, 9,11,12,14,15,16,17-tetradecahydrocyclopenta[a]phenanthren-3-one	DHT	521-18-6
	Testosterone	(8*R*,9*S*,10*R*,13*S*,14*S*,17*S*)-17-hydroxy-10,13-dimethyl-1,2,6,7,8,9,11,12, 14,15,16,17-dodecahydrocyclopenta[a]phenanthren-3-one	Testo	58-22-0
Mild analgesics and precursors	Paracetamol	*N*-(4-hydroxyphenyl)acetamide	Para	103-90-2
	Aspirin	2-acetyloxybenzoic acid	ASA	50-78-2
	Ibuprofen	2-[4-(2-methylpropyl)phenyl]propanoic acid	Ibu	15687-27-1
	Aniline	Benzenamine	Ani	62-53-3
Polyfluorinated compounds	Perfluorooctanesulfonic acid	1,1,2,2,3,3,4,4,5,5,6,6,7,7,8,8,8-heptadecafluorooctane-1-sulfonic acid	PFOS	1763-23-1
	Perfluorooctanoic acid	2,2,3,3,4,4,5,5,6,6,7,7,8,8,8-pentadecafluorooctanoic acid	PFOA	335-67-1

Note: CAS, Chemical Abstracts Service registry; IUPAC, International Union of Pure and Applied Chemistry; UV, ultraviolet.

Wallis test when three groups were compared. Statistical analyses were performed using GraphPad Prism (version 9.0.0; GraphPad Software). Based on the best fit, the equation $Y = \text{Bottom} + (\text{Top-Bottom})/(1+10^{(\text{LogEC}_{50}-X)})$ or $Y = \text{Bottom} + (\text{Top-Bottom})/(1+10^{((\text{LogEC}_{50}-X)\times\text{HillSlope})})$, in GraphPad Prism 9 (GraphPad Software) was used to fit the effective concentration (EC_{50}) curves. Graphs for calcium imaging and *ex vivo* CGRP release studies were prepared using RStudio Team (2016; RStudio: Integrated Development for R. RStudio, Inc.; http://www.rstudio.com/). Graphs for patch clamp, *ex vivo* vasoactivity, von Frey, and motor function studies were prepared in GraphPad Prism (version 9.0.0; GraphPad Software). The significance level was set to 95%, and $p < 0.05$ was considered statistically significant. Statistically significant differences were denoted with asterisks as follows: $^{*} = p < 0.05$, $^{**} = p < 0.01$, $^{***} = p < 0.001$, and $^{****} = p < 0.0001$.

Data Availability

Data supporting the findings in the present study are presented in the article and in supplementary materials. Raw data are available on reasonable request to the corresponding author.

Results

Screen of hTRPA1 and hTRPV1 Activation

To examine whether environmental pollutants could activate hTRPA1 and hTRPV1 channels, we screened a chemical library of 34 chemicals (Table 1) using hTRPA1-HEK, hTRPV1-HEK, and control cell lines. The chemicals tested were part of an already established chemical library developed by coauthor D.M.K. Because TRPA1 and TRPV1 are calcium-permeable ion channels, calcium imaging was used to measure channel activation. The cell lines were initially tested for selective responsiveness to the TRPA1 agonist supercinnamaldehyde (SCA) and the TRPV1 agonist capsaicin to confirm expression of each ion channel (Figure 1A). The cell lines were acutely exposed to 100 μM of each chemical, and the resulting calcium flux was measured for 70 s. hTRPV-HEK1 cells did not differ from control cells in response to any of the individually tested chemicals (Figure 1A). In contrast, higher levels of intracellular calcium $[Ca^{2+}]_i$ was measured in hTRPA1-HEK cells in comparison with control cells when exposed to 10 of the chemicals (Figure 1A). The chemicals resulting in the most pronounced differences were benzyl paraben (BzPa) and the estrogenic compound nonyl phenol (NNP), where exposure resulted in a calcium response of 34.2% (±8.6 SD) and 29.9% (±6.6 SD) relative to the ionomycin positive control (10 μM), in comparison with 0.9% (±0.3 SD) and 0.7 (±0.7 SD) in control cells, respectively. Furthermore, the highly debated chemical bisphenol A (BPA)[44] was found to cause a calcium response of 11.0% (±8 SD) relative to ionomycin in hTRPA1-HEK cells in comparison with control cells 0.1% (±0.2 SD). In addition, a pesticide screen of 18 pesticides (Table 2) was conducted with a lower concentration of 10 μM because of potential toxic effects. The pesticides tested were screened because they were part of an established pesticide library developed by coauthor

Table 2. List of chemicals used for pesticide screen.

Group	Common name	IUPAC name	Abbreviation	CAS number
Pesticides or metabolites	Chlorpyrifos	diethoxy-sulfanylidene-(3,5,6-trichloropyridin-2-yl)oxy-λ^5-phosphane	—	2921-88-2
	Prosulfocarb	*S*-benzyl *N*,*N*-dipropylcarbamothioate	—	52888-80-9
	Fipronil sulfone	5-amino-1-[2,6-dichloro-4-(trifluoromethyl)phenyl]-4-(trifluoromethylsulfonyl)pyrazole-3-carbonitrile	—	120068-36-2
	Trifluralin	2,6-dinitro-*N*,*N*-dipropyl-4-(trifluoromethyl)aniline	—	1582-09-8
	Endosulfan	1,9,10,11,12,12-hexachloro-4,6-dioxa-5λ^4-thiatricyclo[7.2.1.0^{2,8}]dodec-10-ene5-oxide	—	115-29-7
	Hexachlorophene	3,4,6-trichloro-2-[(2,3,5-trichloro-6-hydroxyphenyl)methyl]phenol	HCP	70-30-4
	Imazalil	1-[2-(2,4-dichlorophenyl)-2-prop-2-enoxyethyl]imidazole	—	35554-44-0
	Oxadiazon	5-*tert*-butyl-3-(2,4-dichloro-5-propan-2-yloxyphenyl)-1,3,4-oxadiazol-2-one	—	19666-30-9
	Lindane	1,2,3,4,5,6-hexachlorocyclohexane	—	58-89-9
	Pentachlorophenol	2,3,4,5,6-pentachlorophenol	PCP	87-86-5
	Prochloraz	*N*-propyl-*N*-[2-(2,4,6-trichlorophenoxy)ethyl]imidazole-1-carboxamide	—	67747-09-5
	Cypermethrin	[cyano-(3-phenoxyphenyl)methyl] 3-(2,2-dichloroethenyl)-2,2-dimethylcyclopropane-1-carboxylate	—	52315-07-8
	Permethrin	(3-phenoxyphenyl)methyl 3-(2,2-dichloroethenyl)-2,2-dimethylcyclopropane-1-carboxylate	—	52645-53-1
	Deltamethrin	[(*S*)-cyano-(3-phenoxyphenyl)methyl] (1*R*,3*R*)-3-(2,2-dibromoethenyl)-2,2-dimethylcyclopropane-1-carboxylate	—	52918-63-5
	Boscalid	2-chloro-*N*-[2-(4-chlorophenyl)phenyl]pyridine-3-carboxamide	—	188425-85-6
	Permethric acid	3-(2,2-dichloroethenyl)-2,2-dimethylcyclopropane-1-carboxylic acid	CL2CA	55701-05-8
	3,5,6-trichloro-2-pyridinol	3,5,6-trichloro-1*H*-pyridin-2-one	TCPy	6515-38-4
	Dieldrin	(1R,4S,4AS,5R,6R,7S,8S,8aR)-1,2,3,4,10,10-hexachloro-1,4,4a,5,6,7,8,8a-octahydro-6,7-epoxy-1,4:5,8-dimethanonaphthalene	DED	60-57-1

Note: —, no data; CAS, CAS, Chemical Abstracts Service registry; IUPAC, International Union of Pure and Applied Chemistry.

A.R. The two screens were conducted sequentially to optimize the workflow because of the difference in concentration. The $[Ca^{2+}]_i$ levels were not different in hTRPV1-HEK cells in comparison with control cells when exposed to the tested pesticides; however, hTRPA1-HEK cells exhibited higher $[Ca^{2+}]_i$ levels in comparison with control cells after treatment with six compounds. In particular, hTRPA1-HEK cells exhibited a pronounced calcium response after exposure to hexachlorophene (HCP) and PCP, with an increase in calcium levels equivalent to 47% (±4.9 SD) and 34% (±4.1 SD) of the ionomycin response (10 μM), respectively, in comparison with 2.9% (±0.5 SD) and 0.9% (±0.8 SD) in control cells (Figure 1B). Because ionomycin is a ionophore and elevates $[Ca^{2+}]_i$ levels without direct activation hTRPA1, we also calculated the $[Ca^{2+}]_i$ levels after exposure to PCP and HCP relative to TRPA1 activation caused by the pharmaceutical TRPA1 agonist SCA (10 μM). We found $[Ca^{2+}]_i$ equivalent to 59% (±2.7 SD) and 43% (±5.3 SD) of the SCA response after exposure to HCP and PCP, respectively (Figure 1C).

We chose to further investigate PCP because this pesticide was found at the third-highest concentration and in 100% of the included women, in a cohort of women from the ELFE French nationwide birth cohort, emphasizing its relevance.[45] We exposed hTRPA1-HEK cells to increasing concentrations of PCP (1–100 μM) for 1 h and measured cell viability after acute chemical exposure and found no differences in viability from vehicle across all exposures (Figure S1).

TRPA1-Dependent Calcium Influx in Cell Lines and Primary Neurons

To validate the effect of PCP directly on hTRPA1 channels, whole-cell currents were measured under voltage clamp conditions in hTRPA1-HEK and control cells (Figure 2A–G). PCP induced a dose-dependent membrane current in hTRPA1-HEK cells with an EC_{50} of 15.05 μM (95% CI: 6.429 μM to 63.19 μM) (Figure 2G). 10 μM PCP induced a 6-fold increase in peak current in comparison with baseline ($p = 0.0031$) which subsequently decreased and following administration of the TRPA1 antagonist HC-030031 (100 μM) currents returned completely to baseline, confirming hTRPA1 activation (Figure 2D–F). PCP had no effect on currents in control cells (Figure 2A–C). Next, we studied TRPA1 channels expressed in mouse trigeminal ganglion (TG) neurons isolated from wild type mice. Stimulation with PCP (10 μM) caused an almost 10-fold increase in the current in comparison with baseline ($W = 55.00$; $p = 0.0020$) (10 out of 15 cells). As with TRPA1 currents in hTRPA1-HEK cells, the current in TG neurons subsequently decreased to baseline (Figure 2H–I).

Molecular Modeling of TRPA1 Lipid Binding Pocket

An *in-silico* docking study of PCP in a 3D model of hTRPA1 was made to test whether PCP could activate hTRPA1 by binding in the same lipid pocket as the TRPA1 agonist GNE551. The docking analysis suggested that PCP could be stabilized in this pocket through a polar interaction with E864, thereby potentially facilitating channel opening (Figure 3A,B). A similar docking study of PCP in a hTRPV1 structural model suggested that PCP binds into the lipid pocket of hTRPV1 through hydrophobic interactions, but the residue corresponding to E864 in hTPRA1 (E570) was not reached by PCP. This structural difference between the localization of E864 in hTRPA1 and E570 in hTRPV1 might explain why PCP did not facilitate opening of hTRPV1 (Figure 3C). E570 was not present in the 2D representation because it was too far from PCP in the binding site. The binding affinity scores from the docking analysis in the lipid pockets showed that the estimation for hTRPA1 was −4.36 and −4.17 for hTRPV1, suggesting that the affinity of PCP is slightly higher for hTRPA1.

Because the environmental pollutant acrolein has previously been described as a TRPA1 activator,[8–11] we next *in silico* docked acrolein into hTPRA1 and hTRPV1. The affinity scores for acrolein were weaker in comparison with the scores for PCP (−2.93 for hTRPA1 and −3.7 for hTRPV1). The higher affinity for hTRPV1 might be related to the electrophilic nature of acrolein that mediated a favorable interaction with the binding pocket and stabilization with positive-charged residues such as, for example, R559 (Figure S2). Similar interactions were not identified for the docking into hTRPA1.

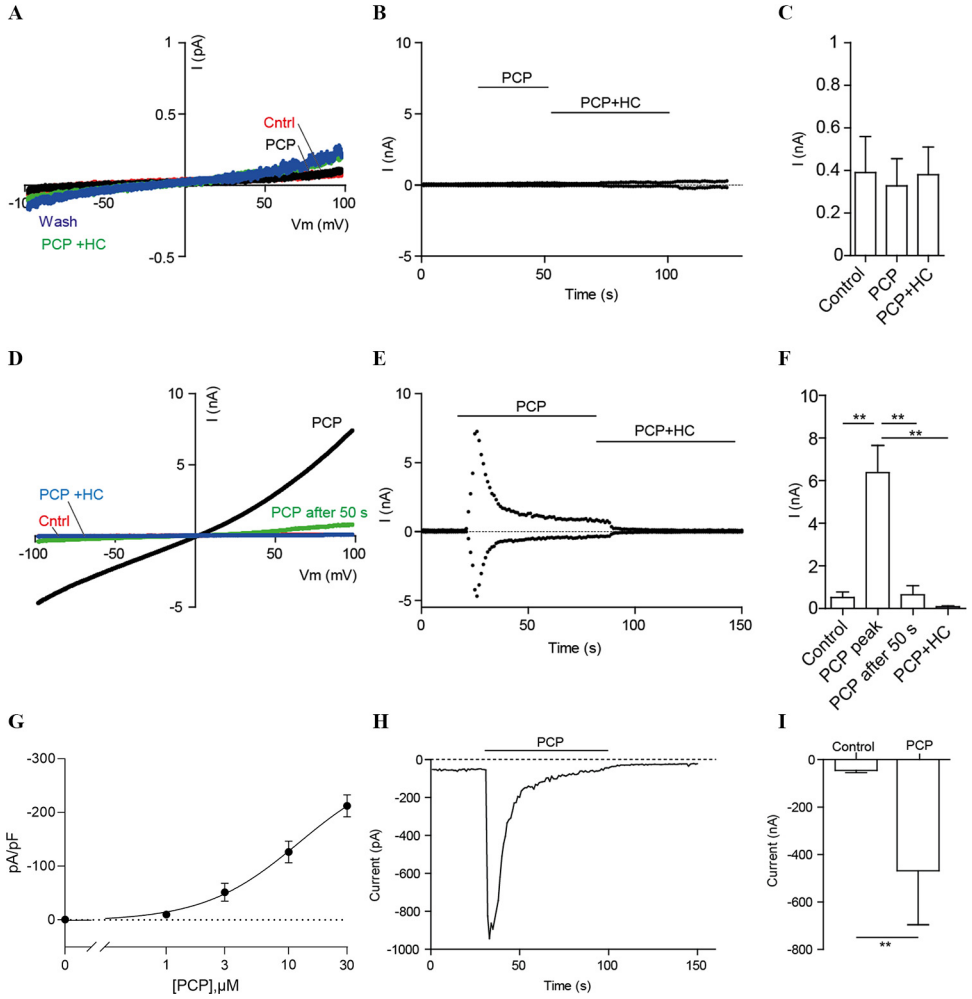

Figure 2. Whole-cell patch clamp recordings from hTRPA1-HEK cells, control cells and neurons isolated from the mouse trigeminal ganglion. Whole-cell voltage clamp recordings using a MultiClamp 700B amplifier and MultiClamp Commander. Currents were activated using a voltage ramp protocol from −100 to +100 mV over 325 ms from a holding potential of −60 mV. Recordings were performed at 36°C in control cells (A–C) and hTRPA1-HEK cells (D–F). (A) Representative currents recorded for control cells elicited by a ramp from −100 to 100 mV in absence and presence of 10 µM PCP and 10 µM PCP+100 µM HC-030031 (HC) (TRPA1 antagonist). (B) A representative current recording from control cells. The current amplitude at −100 and 100 mV is shown as a function of time and in absence and presence of 10 µM PCP as well as 10 µM PCP+100 µM HC. (C) Mean current amplitude (±SEM) in control cells at 100 mV in absence and presence of 10 µM PCP and 10 µM PCP+100 µM HC ($n=4$). One-way ANOVA followed by Bonferroni's multiple comparisons test. Numeric data are found in Table S5. (D) Representative currents recorded from hTRPA1-HEK cells elicited by a ramp from −100 to 100 mV in absence and presence of 10 µM PCP and 10 µM PCP+100 µM HC. (E) Currents recorded from hTRPA1-HEK cells using a ramp from −100 to 100 mV over 325 ms from a holding potential of –60 mV. The current amplitude at −100 and 100 mV is shown as a function of time and in absence and presence of 10 µM PCP as well as 10 µM PCP+100 µM HC. (F) Mean current amplitude (±SEM) in TRPA1- HEK at 100 mV in absence and presence of 10 µM PCP and 10 µM PCP+100 µM HC ($n=3$). One-way ANOVA followed by Bonferroni's multiple comparisons test. Numeric data are found in Table S5. (G) Membrane currents at −60 mV from hTRPA1-HEK cells with the indicated PCP concentrations [EC_{50} of 15.05 µM (95% CI: 6.429 µM to 63.19 µM)] ($n=3$–6). (H) Representative whole-cell current recording of a mouse trigeminal ganglia neuron exposed to 10 µM PCP. The current was measured at a constant voltage of −60 mV. (I) Mean current amplitude (±SEM) in neurons in absence or presence of 10 µM PCP ($n=10$). Wilcoxon matched-pairs signed rank test. Numeric data are found in Table S6. The current measurements of the mouse trigeminal ganglia neurons were performed at 22°C at a constant potential of −60 mV. $^{*}p<0.05$, $^{**}p<0.01$, $^{***}p<0.001$, $^{****}p<0.0001$. Note: ANOVA, analysis of variance; PCP, pentachlorophenol; SEM, standard error of the mean.

TRPA1-Dependent CGRP Release from Mouse TNC

TRPA1 is expressed in peripheral and central terminals of TG neurons and in the postsynaptic dendrites in the TNC, where activation of TRPA1 can lead to release of CGRP.[16,25,46] Release of CGRP is associated with mechanisms involved in migraine attacks[17] and causes vasodilation.[47] In this set of experiments, we examined TRPA1-dependent release of CGRP from the TNC. We first exposed mouse TNC to increasing concentrations of the TRPA1 agonist SCA and found a significant 9-fold increase in CGRP release with 100 µM SCA ($p=0.033$) in comparison with vehicle (0.1% DMSO) (Figure 4A). In TNC from *Trpa1*$^{-/-}$ mice, SCA did not cause significant release of CGRP in comparison with vehicle at any concentration (Figure 4B). PCP similarly caused a significant release of CGRP with a 2- and 5-fold increase at 10 µM ($p=0.0005$) and 100 µM ($p=0.028$), respectively, in comparison with vehicle (0.01% and 0.1% DMSO) (Figure 4C). To verify that the response to PCP was mediated by TRPA1, the experiment was repeated on TNC from *Trpa1*$^{-/-}$ mice. As shown in Figure 4D, the PCP-induced CGRP release was absent in TNC from *Trpa1*$^{-/-}$ mice.

TRPA1-Dependent Dilation of Cerebral Blood Vessels

To validate the functional consequence of CGRP release, we next investigated the ability of PCP to cause dilation of the basilar artery

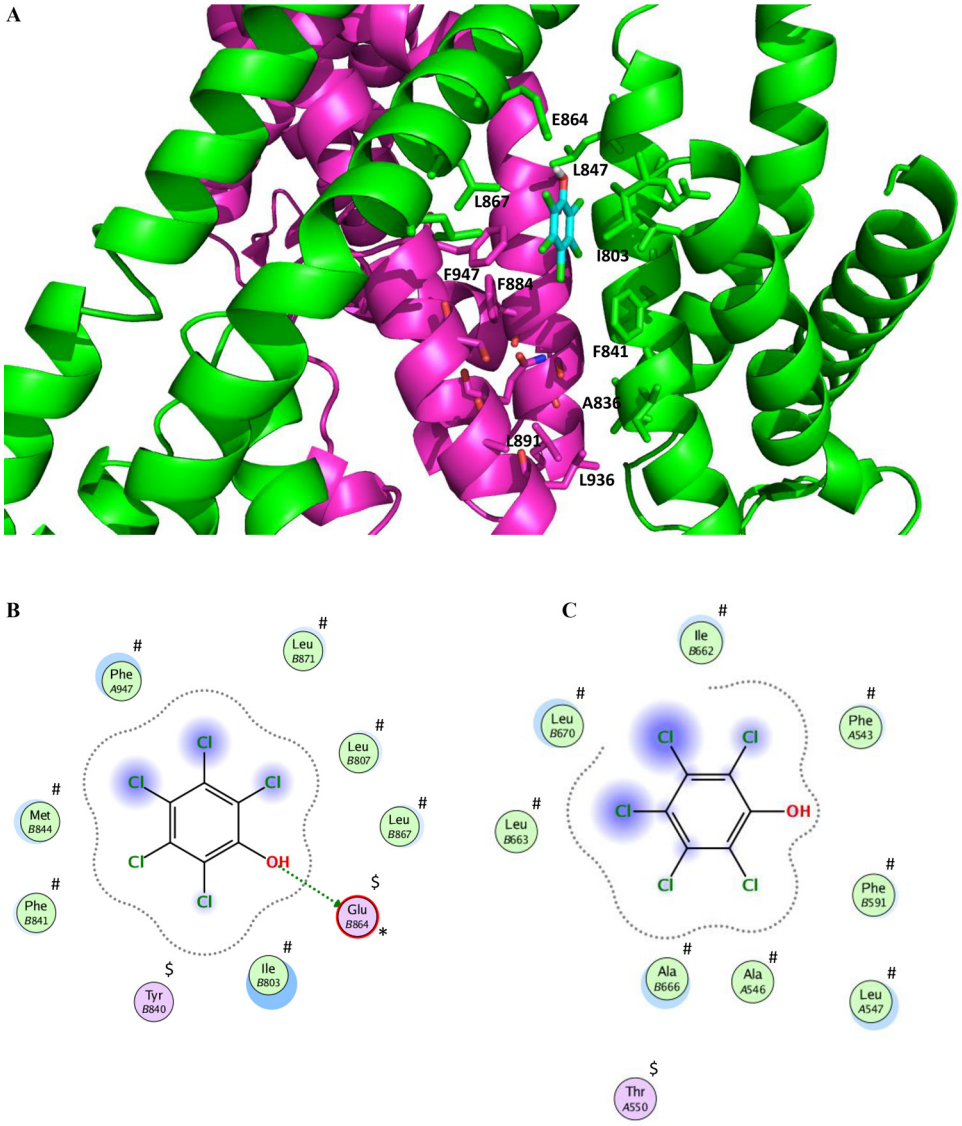

Figure 3. Molecular modeling of pentachlorophenol in lipid pocket of hTRPA1 and hTRPV1. (A) 3D representation of PCP in the lipid pocket of hTRPA1. Two monomeres of hTRPA1 are represented in green and magenta. The PCP is colored in cyan. (B) 2D representation of the docking pose of PCP in hTRPA1. PCP is stabilized through a polar interaction with E864 (green arrow). (C) 2D representation of the docking pose of PCP in hTRPV1. E570 is not present in the 2D representation, because it is located too far from PCP in the binding site. (B–C) The pink spheres are polar residues ($) [with a red border for acidic (*)]. The green spheres are hydrophobic residues (#). The blue shadows are ligand exposure and receptor exposure. The green arrows are hydrogen bond interactions. Note: PCP, pentachlorophenol.

(BA). Following a U46619-induced precontraction (0.3 μM), acute PCP exposure caused a concentration-dependent dilation of the BA [EC_{50} = 2.459 μM (95% CI: 1.996 μM to 2.979 μM)]. BA from *Trpa1*$^{-/-}$ mice required more than a 10-fold higher concentration of PCP to reach a vasodilation comparable to wild type mice. Thus, a clear shift in the concentration-response curve was observed in *Trpa1*$^{-/-}$ mice [EC_{50} = 32.26 μM (95% CI: 12.07 μM to ∞)] in comparison with wild type mice. Accordingly, PCP exposure caused a significantly different vasodilation in *Trpa1*$^{-/-}$ mice compared with wild type mice at 3 μM ($p < 0.0001$) and 10 μM ($p < 0.0001$) (Figure 4E). Treating BA from wild type mice with the migraine-preventive drug (fremanezumab; TEVA Pharmaceutical Industries Ltd.) that inhibits CGRP function[48] caused a slight shift in the concentration–response curve [EC_{50} = 4.818 μM (95% CI: 2.933 μM to 42.16 μM)]. The CGRP ab significantly inhibited the vasodilation caused by PCP at 3 μM ($p = 0.033$) as compared with control BA (Figure 4E).

TRPA1-Dependent Hypersensitivity in Mice as Model of Migraine-like Pain

Finally, we investigated whether PCP could induce tactile hypersensitivity *in vivo* in wild type mice. Tactile sensitivity to stimulation with von Frey monofilaments in the hind paw was used as a surrogate measure of pain and central sensitization.[34,37] Following oral administration of PCP (15 mg/kg), the 50% withdrawal threshold was significantly reduced after 2 h ($p = 0.04$) in comparison with vehicle treatment and marginally at 4 h ($p = 0.06$) (Figure 5A). Figure 5B demonstrates the 50% withdrawal thresholds measured prior to daily PCP administration (basal response). The basal response decreased significantly after 7 d of exposures, on days 8 ($p = 0.045$) and 10 ($p = 0.049$) (Figure 5B). PCP had no effect on motor function 2 h after administration because median time spent on the rotarod was 150 s for both the vehicle (95% CI: 87, 150) and

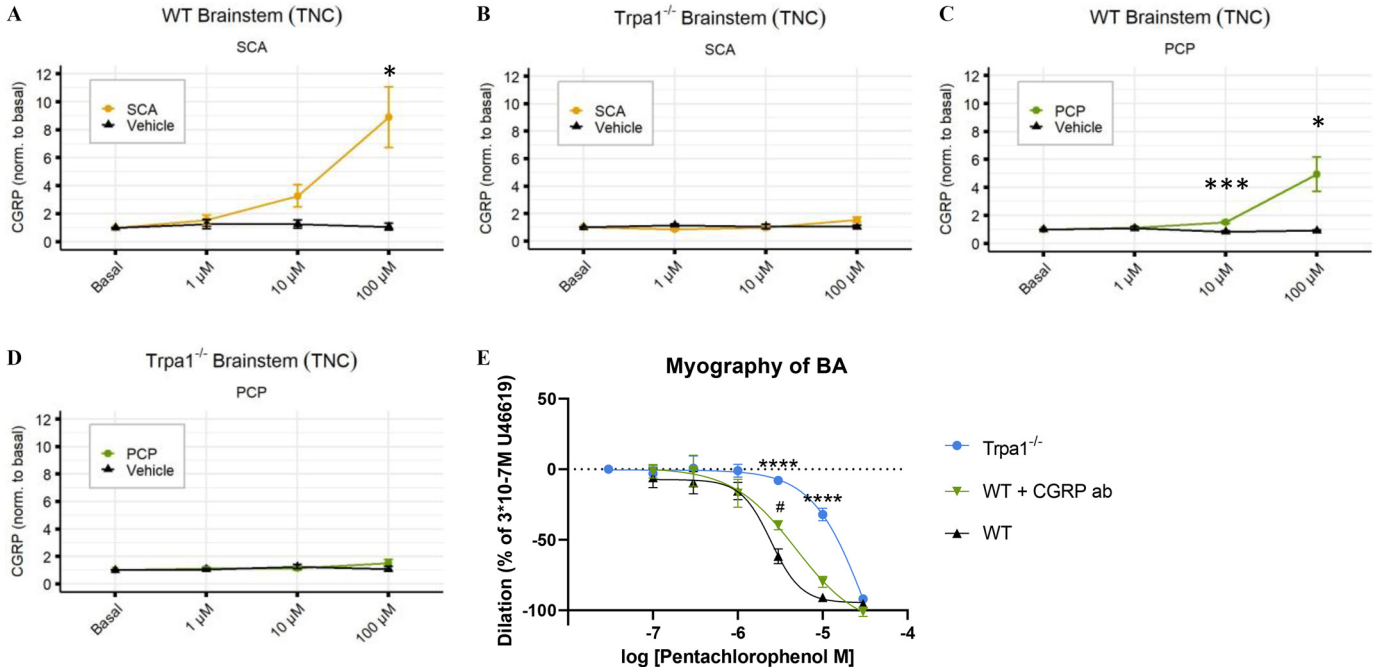

Figure 4. CGRP release from trigeminal nucleus caudalis of wild type and *Trpa1*$^{-/-}$ mice after supercinnamaldehyde, PCP, and vehicle treatment. (A–D) The TNC from WT and *Trpa1*$^{-/-}$ mice was isolated and washed before incubation (37°C) with increasing concentrations of either SCA (A–B) or PCP (C–D) and corresponding vehicle treatment. Following 10 min of incubation, a sample was collected and the released CGRP amount was measured by ELISA. (A–B) CGRP release after increasing concentrations (1 µM, 10 µM, and 100 µM) of SCA (yellow circle) and vehicle (0.1%, 0.01% and 0.001% DMSO) (black triangle) from the TNC from (A) WT (SCA: $n=7$, vehicle: $n=6$) and (B) *Trpa1*$^{-/-}$ mice (SCA: $n=6$, vehicle: $n=6$). Numeric data are found in Tables S7–S8. (C–D) CGRP release from the TNC from (C) WT (PCP: $n=8$, vehicle: $n=6$) and (D) *Trpa1*$^{-/-}$ mice (PCP: $n=7$, vehicle: $n=6$) after stimulation with increasing concentrations (1 µM, 10 µM, and 100 µM) of PCP (green circle) and vehicle (0.1%, 0.01% and 0.001% DMSO) (black triangle). Numeric data are found in Tables S9–S10. (A–D) Data are normalized to the basal response and presented as mean CGRP release with SEMs. Nonnormalized data are found in Tables S11–S14. Multiple unpaired *t* tests with post hoc Holm-Šidák correction. (E) The BA was isolated from WT and *Trpa1*$^{-/-}$ mice following mounting on wire myographs. Dilation of the BA shown as percent of precontraction to increasing concentrations of PCP (10^{-7}M, 3×10^{-7}M, 10^{-6}M, 3×10^{-6}M, 10^{-5}M, and 3×10^{-5}M) from WT (black triangle, $n=4$) and *Trpa1*$^{-/-}$ mice (blue circle, $n=4$), and in presence of 1 µM antibodies directed against human CGRP (CGRP ab) (green upside-down triangle, $n=4$) from WT mice. Numeric data are found in Table S15. Two-way ANOVA. $^{*}p<0.05$, $^{**}p<0.01$, $^{***}p<0.001$, $^{****}p<0.0001$. Note: ANOVA, analysis of variance; BA, basal artery; CGRP, calcitonin gene-related peptide; ELISA, enzyme-linked immunosorbent assay; PCP, pentachlorophenol; SCA, supercinnamaldehyde; SEM, standard error of the mean; TNC, trigeminal nucleus caudalis; WT, wild type.

PCP (95% CI: 90, 150) group ($p=0.97$) and 44.5 s in the midazolam positive control group (95% CI: 34, 53) ($p<0.0001$) (Figure 5C).

To confirm our findings and to test whether this response was dependent on TRPA1, we repeated the experiment both in wild type and *Trpa1*$^{-/-}$ mice. PCP administration (15 mg/kg p.o.) in wild type mice reduced the 50% withdrawal threshold significantly 2 h after administration in comparison with vehicle treatment ($p<0.0001$). The effect was more pronounced in comparison with the first experiment, with PCP reducing the 50% withdrawal threshold significantly ($p=0.0004$) after 4 h, too. In *Trpa1*$^{-/-}$ mice, PCP administration did not change the 50% withdrawal threshold in comparison with vehicle treatment at 2 h ($p=0.82$) or 4 h ($p=0.38$) (Figure 5D). PCP had no effect on motor function in *Trpa1*$^{-/-}$ mice at 2 h or 4 h after administration because median time spent on the rotarod was 150 s at both time points for vehicle-treated *Trpa1*$^{-/-}$ mice (2 h: 95% CI: 136, 150 and 4 h: 95% CI: 150, 150), PCP-treated *Trpa1*$^{-/-}$ mice (2 h: 95% CI: 150, 150 and 4 h: 95% CI: 150, 150) and wild type mice (2 h: 95% CI: 150, 150 and 4 h: 95% CI: 150, 150). The midazolam-treated positive control group was significantly different from the control saline group ($p<0.0001$), with the median time spent on the rotarod of 38 s in the midazolam group (95% CI: 32, 42) and 150 s in the saline group (95% CI: 150, 150) (Figure 5E).

Discussion

The data presented in this study indicate that various environmental chemicals, including pesticides and parabens, have the potential to activate TRPA1, leading to increased intracellular calcium levels. Examining the pesticide PCP, we validated activation of heterologous expressed TRPA1 in HEK cells using whole-cell path clamp recordings and found that PCP increased currents in primary mouse TG neurons. These findings were supported by *in silico* modeling, which suggested that the ability of PCP to activate TRPA1 might be attributed to its polar interaction with E864 and a slightly higher affinity for the lipid pocket, distinguishing it from TRPV1 activation. Collectively, these experiments also propose that PCP exposure causes release of CGRP from peptidergic neurons, leading to blood vessel dilation, and that vessel dilation is dependent on the activation of TRPA1 and the release of CGRP. Moreover, *in vivo* experiments collectively support a mechanism by which PCP induced hypersensitivity through stimulation of TRPA1 in mice. Overall, we showed using an *in vitro* and *in vivo* approach that the trigeminovascular pain circuit is a potential target for environmental chemicals. The proposed mechanism is a TRPA1-dependent CGRP release from neurons in the trigeminovascular system, causing vasodilation and sensitization which ultimately leads to increased pain perception (Figure 6), as previously described for the naturally occurring chemical umbellulone.[16]

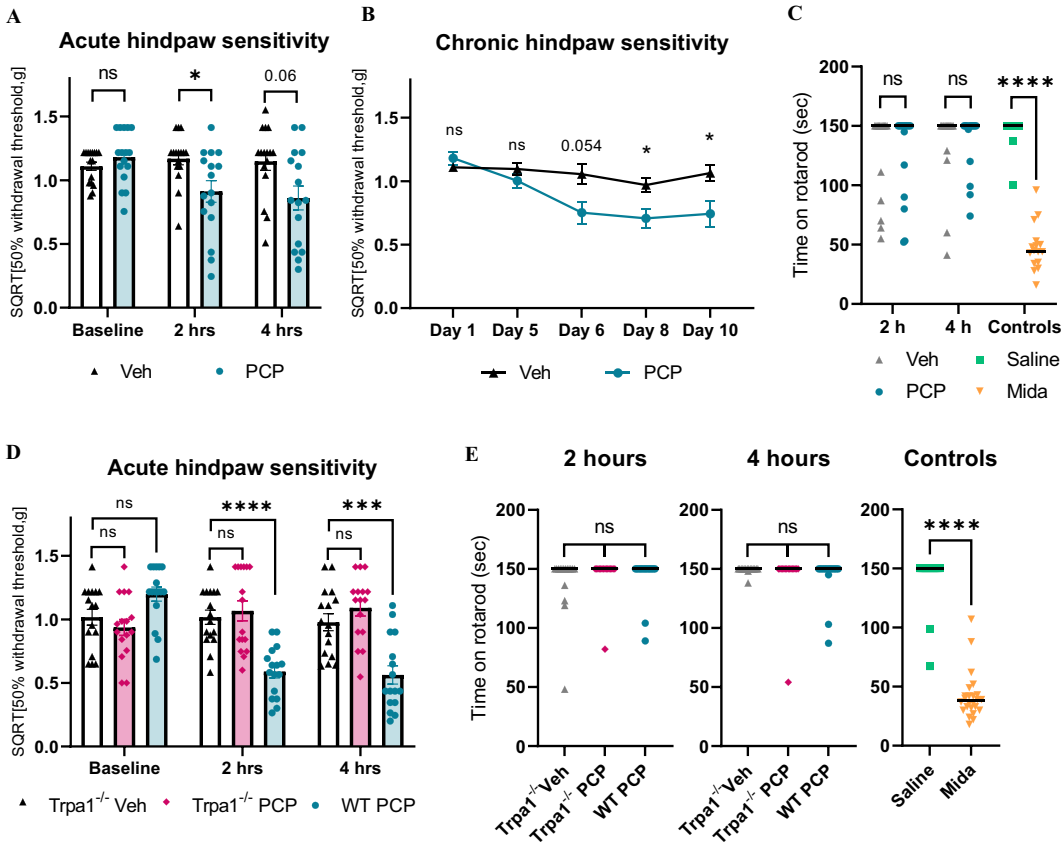

Figure 5. Acute and chronic hind-paw sensitivity and motor function in mice treated with PCP or vehicle. Acute and chronic sensitivity to tactile stimulation on the plantar area is measured with von Frey filaments. Acute hypersensitivity (A, D) was measured 2 h and 4 h post drug administration, whereas chronic hypersensitivity (B) was measured the following day prior to drug administration. On completion of the von Frey experiments, the motor function of the mice was examined using a rotarod where the time spent on a horizontal rotating rod was measured. Mice were placed on the rotarod with a start speed of 0 rpm, which was increased to 30 rpm with a ramp of 45 s and terminated after 150 s. The first cohort of mice is presented in A–C, and the second cohort including *Trpa1*$^{-/-}$ mice is presented in D–E. (A) Acute effect 2 h and 4 h post PCP (15 mg/kg p.o. in 0.5% CMC in water, $n = 16$) (blue circle) or Veh (p.o., $n = 16$) (black triangle) administration in WT mice. Sensitivity was measured with von Frey filaments and calculated as 50% withdrawal threshold (g). Two-way ANOVA with Šidák's test. (B) Basal response (before PCP administration) in WT mice following daily administration of PCP (15 mg/kg p.o. in 0.5% CMC in water, $n = 16$) or vehicle (p.o., $n = 16$) for 10 d. Sensitivity was measured with von Frey filaments and calculated as 50% withdrawal threshold (g). Two-way ANOVA with Šidák's test. (C) Locomotor performance was tested using a rotarod. The time spent on a rotating rod was measured in seconds, with a maximal duration of 150 s. Motor function was examined 2 and 4 h after PCP ($n = 16$) or Veh ($n = 16$) administration and 10 min after (Mida) (i.p. $n = 16$) or saline (i.p., $n = 16$) administration in WT mice. Data are presented as individual data points and medians. Multiple Mann-Whitney tests with Holm-Šidák post hoc comparison (D) Acute effect 2 h and 4 h post PCP (15 mg/kg p.o. in 0.5% CMC in water, $n = 16$) or vehicle (p.o., $n = 16$) administration in WT and *Trpa1*$^{-/-}$ mice. Sensitivity was measured with von Frey filaments and calculated as 50% withdrawal threshold (g). Two-way ANOVA with post hoc Dunnett's correction. (E) Locomotor performance was tested using a rotarod. The time spent on a rotating rod was measured in seconds with a maximal duration of 150 s. Motor function was examined 2 and 4 h after PCP ($n = 16$) or vehicle ($n = 16$) administration in WT and PCP ($n = 16$) administration *Trpa1*$^{-/-}$ mice, and 10 min after Mida (i.p., $n = 24$) or saline (i.p., $n = 24$) administration. Data are presented as individual data points and medians. Kruskal-Wallis with Dunn's post hoc test for 2 h and 4 h data and Mann-Whitney for controls. (A, D) Data are presented as individual data points with means ± SEMs and calculated as 50% withdrawal threshold (g) after SQRT. (B) Data are presented as means ± SEMs and calculated as 50% withdrawal threshold (g) after SQRT. Numeric data for A–E is found in Tables S16–S20. $^{*}p < 0.05$, $^{**}p < 0.01$, $^{***}p < 0.001$, $^{****}p < 0.0001$. Note: ANOVA, analysis of variance; Mida, midazolam; PCP, pentachlorophenol; SEM, standard error of the mean; SQRT, square root transformation; Veh, vehicle; WT, wild type.

Modeling data suggested that PCP can activate TRPA1 through stabilization in the lipid binding pocket across a specific polar interaction with E864. Although TRPV1 and TRPA1 share a high degree of structural homology in the transmembrane region,[26,49] only TRPA1 was found to be promiscuous. Comparing TRPA1 agonist GNE551 complexed in the lipid pocket of TRPA1 with that of TRPV1 agonist capsaicin in the pocket of TRPV1 led us to conclude that E864 of TRPA1 is conserved as E570 in TRPV1.[49] Previous data showed that the interaction of TRPV1 with agonist capsaicin led to the displacement of a lipid in the binding pocket, facilitating the channel opening through a rearrangement of transmembrane helices and a stabilization of an interaction between residue R557 of one helix and residue E570 of the second helix.[49] The E570 residue formed polar interactions with the head group of the resident lipids in the closed state and was involved in activation upon capsaicin binding.[26] Although modeling showed that E864 was reached by PCP in TRPA1, the pesticide could not reach residue E570 in TRPV1, thereby providing a potential mechanism for the selective activation of TRPA1.

PCP was used in proof-of-concept *ex vivo* and *in vivo* experiments. Real life entails simultaneous exposure to multiple environmental chemicals in mixtures that can lead to additive effects at doses where the individual compound may have no effect alone.[50] Among the screened chemicals 30% (16 of 52 chemicals, including pesticides) activated TRPA1. This finding is not surprising, given the promiscuous nature of this channel,[51] and is in line with the observations from other promiscuous related Ca^{2+} channels, e.g., CatSper.[52] Because we investigated only a fraction of the thousands of environmental pollutants ubiquitously present in industrialized regions, it is likely that future studies will identify more chemicals,

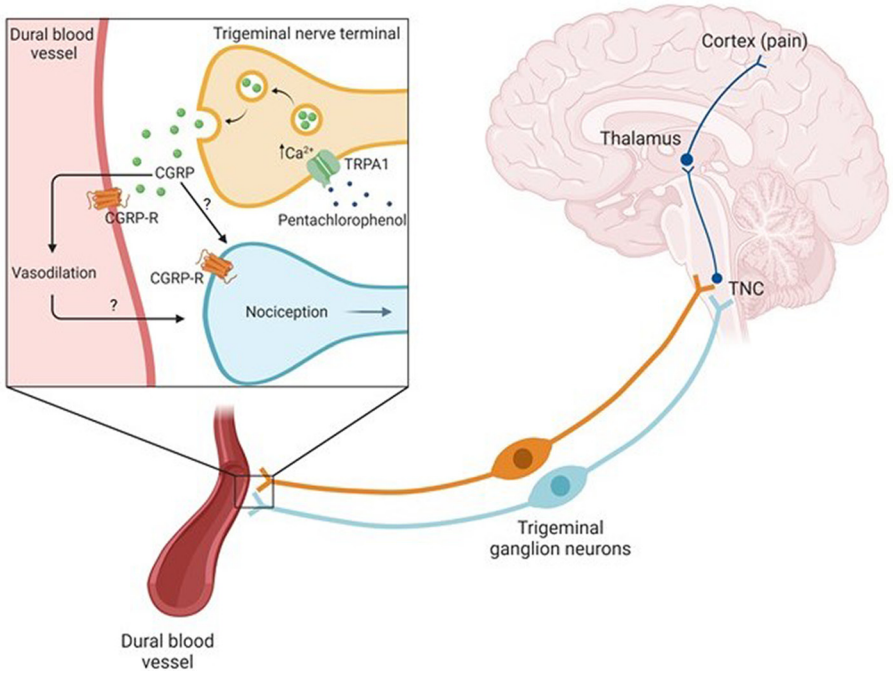

Figure 6. Schematic illustration of the proposed signaling pathway involved in PCP-induced hypersensitivity. Interpretation of data from Figures 1–5. PCP was shown to activate TRPA1 with subsequent release of CGRP, resulting in dilation of blood vessels. PCP administration also induced hypersensitivity in mice via TRPA1. Created with Biorender.com. Note: CGRP, calcitonin gene-related peptide; CGRP-R, CGRP receptor; PCP, pentachlorophenol; TNC, trigeminal nucleus caudalis.

or combinations of chemicals, that trigger TRPA1 and result in release of migraine-inducing neuropeptides such as CGRP.

The effect of PCP alone is concerning. Because of its bactericidal and fungicidal properties, PCP was formerly used widely for impregnation of textiles, as a wood and paint preservative, and as an herbicide in agriculture. Today, PCP is banned in most countries, and blood levels of PCP decreased in Germany between 1989 and 1998.[53] However, the pesticide remains in the environment; a study from southwestern and northeastern France has shown that 100% of the women giving birth included in the study had measurable levels of PCP in hair samples after its ban, and these levels were high in comparison with the other tested pesticides.[45]

In the current study, we used a dose of 15 mg/kg PCP (oral administration) in *in vivo* experiments. Previously, this dose has shown a peak plasma concentration of 28 mg/L in B6C3F1 mice 1.5 h after oral administration.[54] This dose is equivalent to a concentration of ∼100 μM, which resulted in a TRPA1-dependent release of CGRP from trigeminal neurons *ex vivo*. Heudorf et al.[53] found a mean PCP concentration in plasma of 2.4 μg/L, with a maximum value of 59.3 μg/L in people living in Germany in 1998. Other studies have found that individuals with occupational exposure and residents of PCP-treated log homes have plasma/serum levels exceeding 1 mg/L (∼3.75 μM).[53,55,56] When comparing animal exposure studies to human exposure levels, difference in body size needs to be considered. A system of allometry based on the body surface area can be applied where mouse dose data are divided by a factor of 12.33.[57] An alternative approach is to use a 100-fold default uncertainty factor to convert animal experimental levels to "safe" levels for human exposure.[58] When taking such conversion factors into consideration, the peak plasma concentration of 28 mg/L reached in mice in the present study is close to or within the exposure range observed among humans (e.g., 1 mg/L). Moreover, the EC_{50} of 15.05 μM established by patch clamp experiments on hTRPA1-HEK cells strongly suggests that the doses previously identified in humans have no or little margin of safety in relation to activating TRPA1.

TRPA1 has been described as a chemosensor of environmental irritants such as acrolein[59] and formaldehyde,[60] but in general, few environmental chemicals have been investigated in relation to migraine. A connection between environmental irritant–induced TRPA1-activation and pain signaling was described previously by Kunkler et al.,[10] who showed that acrolein induced meningeal vasodilation and release of CGRP from trigeminal neurons. These findings were further supported by data showing that chronic acrolein exposure resulted in sensitization of the trigeminal system[11] and induction of migraine phenotypes in rats.[9] Our data recapitulated a similar scenario for PCP. Another environmental pollutant, the xenoestrogen BPA was found to exacerbate migraine symptoms in a multibehavior model of migraine in ovariectomized rats.[8] Here, BPA exposure was hypothesized to exert its effect on migraine-associated behavior through estrogen signaling, because BPA has estrogenic activity, and estrogen receptors are found in trigeminal neurons and known to be involved in exacerbation of trigeminal pain.[61] In the present study, we showed that BPA was able to activate TRPA1. It cannot be excluded that TRPA1 activation and subsequent CGRP release potentially contribute to the exacerbation of migraine-like behavior in BPA-treated rats. Overall, previous findings together with the present study emphasize that environmental chemicals can interfere with signaling relevant for migraine resulting in migraine-like pain behavior in animal models.

The *in vivo* model of migraine-like pain is based on a reverse translational approach. Numerous prior studies have shown that vasodilating compounds such as glyceryl trinitrate (GTN) and levcromakalim cause migraine,[62,63] and migraine-like pain in mice identified by proxy as cutaneous hypersensitivity to tactile stimulation.[34,35] PCP-induced hypersensitivity was measured by sensitivity to von Frey monofilament in the hind paw with

subsequent calculation of 50% withdrawal thresholds. Measuring hypersensitivity in the periorbital region intuitively appears more relevant when studying a disorder like migraine. However, measurements in both the plantar and periorbital areas are relevant in migraine research because hypersensitivity can be measured in both regions after administration of the migraine triggers GTN,[34] levcromakalim, cilostazol,[42] and pituitary adenylate cyclase-activating polypeptide (PACAP).[43] However, cephalic measurements have greater variability and a more narrow effect window, requiring larger groups of mice.[42,43] Therefore, measurements in the plantar region are the optimal choice to reduce the number of experimental animals. The fact that in this study PCP-exposed cells released CGRP, and PCP exposure was associated with dilation of blood vessels *ex vivo*, emphasizes the pesticide's ability to interfere with migraine-associated tissue responses and signaling. We therefore believe that the hypersensitivity measured after PCP administration is relevant as a surrogate measure of migraine pain. Furthermore, the aforementioned known experimental migraine trigger GTN, which is used to induce migraine in humans[62] and constitutes a well-validated mouse model of migraine after repeated dosing,[34,41,64] was shown to be fully dependent on TRPA1 using both chemical inhibition and genetic deletion of *Trpa1* in mice.[42] This finding emphasizes the importance of TRPA1 in the used models of migraine. To verify that the PCP-induced hypersensitivity is relevant as a measure of migraine pain, future studies investigating PCP-induced hypersensitivity in CGRP deficient mice or in combination with known migraine treatments will be necessary.[37,42,64]

To conclude, we here provide mechanistic evidence for a neurobiological impact of environmental chemicals in relation to migraine signaling. By integrating calcium imaging, patch clamp recordings, *in silico* modeling, *ex vivo* assays, and an *in vivo* mouse model, we found evidence that 16 out of 52 environmental chemicals activated the pain receptor TRPA1. As a proof of concept, our findings also suggested that the pesticide PCP could change pain thresholds as a marker of migraine pain through a TRPA1-CGRP-dependent pathway at physiologically relevant concentrations. These results emphasize the need to further investigate how environmental chemicals alone or in mixtures might change neurobiological signaling pathways related to pain and are relevant for the ongoing debate concerning the possible increasing migraine prevalence.

Acknowledgments

This work was supported by Svend Andersen Fonden, Candys Foundation, Brødrene Hartmanns Fond, Fonden til Lægevidenskabelig Fremme & Torben og Alice Frimodt Fond.

References

1. Vos T, Abajobir AA, Abate KH, Abbafati C, Abbas KM, Abd-Allah F, et al. 2017. Global, regional, and national incidence, prevalence, and years lived with disability for 328 diseases and injuries for 195 countries, 1990–2016: a systematic analysis for the Global Burden of Study 2016. Lancet 390(10100):1211–1259, https://doi.org/10.1016/S0140-6736(17)32154-2.
2. Rozen TD, Swanson JW, Stang PE, McDonnell SK, Rocca WA. 1999. Increasing incidence of medically recognized migraine headache in a United States population. Neurology 53(7):1468–1473, PMID: 10534253, https://doi.org/10.1212/wnl.53.7.1468.
3. Sillanpää M, Piekkala P, Kero P. 1991. Prevalence of headache at preschool age in an unselected child population. Cephalalgia 11(5):239–242, PMID: 1773439, https://doi.org/10.1046/j.1468-2982.1991.1105239.x.
4. Le H, Tfelt-Hansen P, Skytthe A, Kyvik KO, Olesen J. 2012. Increase in self-reported migraine prevalence in the Danish adult population: a prospective longitudinal population-based study. BMJ Open 2(4):e000962–7, https://doi.org/10.1136/bmjopen-2012-000962.
5. Burch R, Rizzoli P, Loder E. 2018. The prevalence and impact of migraine and severe headache in the United States: figures and trends from government health studies. Headache 58(4):496–505, PMID: 29527677, https://doi.org/10.1111/head.13281.
6. Lipton RB, Stewart WF, Diamond S, Diamond ML, Reed M. 2001. Prevalence and burden of migraine in the United States: data from the American Migraine Study II. Headache J Head Face Pain 41(7):646–657, PMID: 11554952, https://doi.org/10.1046/j.1526-4610.2001.041007646.x.
7. Woldeamanuel YW, Cowan RP. 2017. Migraine affects 1 in 10 people worldwide featuring recent rise: a systematic review and meta-analysis of community-based studies involving 6 million participants. J Neurol Sci 372:307–315, PMID: 28017235, https://doi.org/10.1016/j.jns.2016.11.071.
8. Vermeer LMM, Gregory E, Winter MK, McCarson KE, Berman NEJ. 2014. Exposure to bisphenol a exacerbates migraine-like behaviors in a multibehavior model of rat migraine. Toxicol Sci 137(2):416–427, PMID: 24189132, https://doi.org/10.1093/toxsci/kft245.
9. Kunkler PE, Zhang LJ, Johnson PL, Oxford GS, Hurley JH. 2018. Induction of chronic migraine phenotypes in a rat model after environmental irritant exposure. Pain 159(3):540–549, PMID: 29200178, https://doi.org/10.1097/j.pain.0000000000001124.
10. Kunkler PE, Ballard CJ, Oxford GS, Hurley JH. 2011. TRPA1 receptors mediate environmental irritant-induced meningeal vasodilatation. Pain 152(1):38–44, PMID: 21075522, https://doi.org/10.1016/j.pain.2010.08.021.
11. Kunkler PE, Zhang L, Pellman JJ, Oxford GS, Hurley JH. 2015. Sensitization of the trigeminovascular system following environmental irritant exposure. Cephalalgia 35(13):1192–1201, PMID: 25724913, https://doi.org/10.1177/0333102415574845.
12. Bernhardt ES, Rosi EJ, Gessner MO. 2017. Synthetic chemicals as agents of global change. Front Ecol Environ 15(2):84–90, https://doi.org/10.1002/fee.1450.
13. Bennett D, Bellinger DC, Birnbaum LS, Bradman A, Chen A, Cory-Slechta DA, et al. 2016. Project TENDR: Targeting Environmental Neuro-Developmental Risks. The TENDR Consensus Statement. Environ Health Perspect 124(7):A118–A122, PMID: 27479987, https://doi.org/10.1289/EHP358.
14. Drake ME, Stuhr ET. 1935. Some pharmacological and bactericidal properties of umbellulone. J Am Pharm Assoc 24(3):196–207, https://doi.org/10.1002/jps.3080240304.
15. Peattie DC. 2017. *A Natural History of Western Trees*. Boston, MA: Houghton Mifflin Co.
16. Nassini R, Materazzi S, Vriens J, Prenen J, Benemei S, De Siena G, et al. 2012. The 'headache tree' via umbellulone and TRPA1 activates the trigeminovascular system. Brain 135(pt 2):376–390, PMID: 22036959, https://doi.org/10.1093/brain/awr272.
17. Edvinsson L. 2017. The trigeminovascular pathway: role of CGRP and CGRP receptors in migraine. Headache 57 Suppl 2:47–55, PMID: 28485848, https://doi.org/10.1111/head.13081.
18. Edvinsson L, Haanes KA, Warfvinge K, Krause DN. 2018. CGRP as the target of new migraine therapies – successful translation from bench to clinic. Nat Rev Neurol 14(6):338–350, PMID: 29691490, https://doi.org/10.1038/s41582-018-0003-1.
19. Oxford GS, Hurley JH. 2013. The role of TRP channels in migraine. Open Pain J 6(1):37–49, https://doi.org/10.2174/1876386301306010037.
20. Iannone LF, De Logu F, Geppetti P, De Cesaris F. 2022. The role of TRP ion channels in migraine and headache. Neurosci Lett 768:136380, PMID: 34861342, https://doi.org/10.1016/j.neulet.2021.136380.
21. Materazzi S, Benemei S, Fusi C, Gualdani R, De Siena G, Vastani N, et al. 2013. Parthenolide inhibits nociception and neurogenic vasodilatation in the trigeminovascular system by targeting TRPA1 channel. Pain 154(12):2750–2758, PMID: 23933184, https://doi.org/10.1016/j.pain.2013.08.002.
22. Mata-Martínez E, José O, Torres-Rodríguez P, Solís-López A, Sánchez-Tusie AA, Sánchez-Guevara Y, et al. 2013. Measuring intracellular Ca2+ changes in human sperm using four techniques: conventional fluorometry, stopped flow fluorometry, flow cytometry and single cell imaging. J Vis Exp (75):e50344, PMID: 23728309, https://doi.org/10.3791/50344.
23. Yoo S, Choi S-I, Lee S, Song J, Yang C, Bang S, et al. 2017. Endogenous TRPV4 expression of a hybrid neuronal cell line N18D3 and its utilization to find a novel synthetic ligand. J Mol Neurosci 63(3–4):422–430, PMID: 29090425, https://doi.org/10.1007/s12031-017-0993-y.
24. Benemei S, De Logu F, Li Puma S, Marone IM, Coppi E, Ugolini F, et al. 2017. The anti-migraine component of butterbur extracts, isopetasin, desensitizes peptidergic nociceptors by acting on TRPA1 cation channel. Br J Pharmacol 174(17):2897–2911, PMID: 28622417, https://doi.org/10.1111/bph.13917.
25. Kim YS, Son JY, Kim TH, Paik SK, Dai Y, Noguchi K, et al. 2010. Expression of transient receptor potential ankyrin 1 (TRPA 1) in the rat trigeminal sensory afferents and spinal dorsal horn. J Comp Neurol 518(5):687–698, PMID: 20034057, https://doi.org/10.1002/cne.22238.
26. Liu C, Reese R, Vu S, Rougé L, Shields SD, Kakiuchi-Kiyota S, et al. 2021. A non-covalent ligand reveals biased agonism of the TRPA1 ion channel. Neuron 109(2):273–284.e4, PMID: 33152265, https://doi.org/10.1016/j.neuron.2020.10.014.

27. Caterina MJ, Schumacher MA, Tominaga M, Rosen TA, Levine JD, Julius D. 1997. The capsaicin receptor: a heat-activated ion channel in the pain pathway. Nat 389(6653):816–824, PMID: 9349813, https://doi.org/10.1038/39807.
28. Abdel-Salam OME, Mózsik G. 2023. Capsaicin, the vanilloid receptor TRPV1 agonist in neuroprotection: mechanisms involved and significance. Neurochem Res 48(11):3296–3315, https://doi.org/10.1007/s11064-023-03983-z.
29. Kwon DH, Zhang F, Suo Y, Bouvette J, Borgnia MJ, Lee SY. 2021. Heat-dependent opening of TRPV1 in the presence of capsaicin. Nat Struct Mol Biol 28(7):554–563, PMID: 34239123, https://doi.org/10.1038/s41594-021-00616-3.
30. Kwan KY, Allchorne AJ, Vollrath MA, Christensen AP, Zhang D-S, Woolf CJ, et al. 2006. TRPA1 contributes to cold, mechanical, and chemical nociception but is not essential for hair-cell transduction. Neuron 50(2):277–289, PMID: 16630838, https://doi.org/10.1016/j.neuron.2006.03.042.
31. Rasmussen RH, Jansen-Olesen I, Kristensen DM, Christensen SL. 2022. Ex vivo release of calcitonin gene-related peptide from the trigeminovascular system in rodents. J Vis Exp (183), PMID: 35635478, https://doi.org/10.3791/63723.
32. Mulvany M, Halpern W. 1976. Mechanical properties of vascular smooth muscle cells *in situ*. Nature 260:617–619, https://doi.org/10.1038/260617a0.
33. Mulvany MJ, Halpern W. 1977. Contractile properties of small arterial resistance vessels in spontaneously hypertensive and normotensive rats. Circ Res 41(1):19–26, PMID: 862138, https://doi.org/10.1161/01.res.41.1.19.
34. Pradhan AA, Smith ML, McGuire B, Tarash I, Evans CJ, Charles A. 2014. Characterization of a novel model of chronic migraine. Pain 155(2):269–274, PMID: 24121068, https://doi.org/10.1016/j.pain.2013.10.004.
35. Christensen SL, Munro G, Petersen S, Shabir A, Jansen-Olesen I, Kristensen DM, et al. 2020. ATP sensitive potassium (KATP) channel inhibition: a promising new drug target for migraine. Cephalalgia 40(7):650–664, PMID: 32418458, https://doi.org/10.1177/0333102420925513.
36. Tipton AF, Tarash I, McGuire B, Charles A, Pradhan AA. 2016. The effects of acute and preventive migraine therapies in a mouse model of chronic migraine. Cephalalgia 36(11):1048–1056, PMID: 26682574, https://doi.org/10.1177/0333102415623070.
37. Christensen SL, Petersen S, Kristensen DM, Olesen J, Munro G. 2019. Targeting CGRP via receptor antagonism and antibody neutralisation in two distinct rodent models of migraine-like pain. Cephalalgia 39(14):1827–1837, PMID: 31288556, https://doi.org/10.1177/0333102419861726.
38. Chaplan SR, Bach FW, Pogrel JW, Chung JM, Yaksh TL. 1994. Quantitative assessment of tactile allodynia in the rat paw. J Neurosci Methods 53(1):55–63, PMID: 7990513, https://doi.org/10.1016/0165-0270(94)90144-9.
39. Dixon WJ. 1980. Efficient analysis of experimental observations. Annu Rev Pharmacol Toxicol 20(1):441–462, PMID: 7387124, https://doi.org/10.1146/annurev.pa.20.040180.002301.
40. Christensen SL, Hansen RB, Storm MA, Olesen J, Hansen TF, Ossipov M, et al. 2020. Von Frey testing revisited: provision of an online algorithm for improved accuracy of 50% thresholds. Eur J Pain 24(4):783–790, PMID: 31889375, https://doi.org/10.1002/ejp.1528.
41. Christensen SL, Ernstsen C, Olesen J, Kristensen DM. 2020. No central action of CGRP antagonising drugs in the GTN mouse model of migraine. Cephalalgia 40(9):924–934, PMID: 32223300, https://doi.org/10.1177/0333102420914913.
42. Christensen SL, Rasmussen RH, Ernstsen C, La Cour S, David A, Chaker J, et al. 2021. CGRP-dependent signalling pathways involved in mouse models of GTN-cilostazol- and levcromakalim-induced migraine. Cephalalgia 41(14):1413–1426, PMID: 34407650, https://doi.org/10.1177/03331024211038884.
43. Ernstsen C, Christensen SL, Rasmussen RH, Nielsen BS, Jansen-Olesen I, Olesen J, et al. 2022. The PACAP pathway is independent of CGRP in mouse models of migraine: possible new drug target? Brain 145(7):2450–2460, PMID: 35136961, https://doi.org/10.1093/brain/awac040.
44. Vom Saal FS, Akingbemi BT, Belcher SM, Birnbaum LS, Crain DA, Eriksen M, et al. 2007. Chapel Hill bisphenol Aa expert panel consensus statement: integration of mechanisms, effects in animals and potential to impact human health at current levels of exposure. Reprod Toxicol 24(2):131–138, PMID: 17768031, https://doi.org/10.1016/j.reprotox.2007.07.005.
45. Béranger R, Hardy EM, Dexet C, Guldner L, Zaros C, Nougadère A, et al. 2018. Multiple pesticide analysis in hair samples of pregnant French women: results from the ELFE national birth cohort. Environ Int 120(March):43–53, PMID: 30064054, https://doi.org/10.1016/j.envint.2018.07.023.
46. Benemei S, Fusi C, Trevisan G, Geppetti P. 2014. The TRPA1 channel in migraine mechanism and treatment. Br J Pharmacol 171(10):2552–2567, PMID: 24206166, https://doi.org/10.1111/bph.12512.
47. Brain SD, Grant AD. 2004. Vascular actions of calcitonin gene-related peptide and adrenomedullin. Physiol Rev 84(3):903–934, PMID: 15269340, https://doi.org/10.1152/physrev.00037.2003.
48. Dodick DW, Silberstein SD, Bigal ME, Yeung PP, Goadsby PJ, Blankenbiller T, et al. 2018. Effect of fremanezumab compared with placebo for prevention of episodic migraine. JAMA 319(19):1999–2008, PMID: 29800211, https://doi.org/10.1001/jama.2018.4853.
49. Gao Y, Cao E, Julius D, Cheng Y. 2016. TRPV1 structures in nanodiscs reveal mechanisms of ligand and lipid action. Nature 534(7607):347–351, PMID: 27281200, https://doi.org/10.1038/nature17964.
50. Kortenkamp A. 2014. Low dose mixture effects of endocrine disrupters and their implications for regulatory thresholds in chemical risk assessment. Curr Opin Pharmacol 19:105–111, PMID: 25244397, https://doi.org/10.1016/j.coph.2014.08.006.
51. Talavera K, Startek JB, Alvarez-Collazo J, Boonen B, Alpizar YA, Sanchez A, et al. 2020. Mammalian transient receptor potential TRPA1 channels: from structure to disease. Physiol Rev 100(2):725–803, PMID: 31670612, https://doi.org/10.1152/physrev.00005.2019.
52. Schiffer C, Müller A, Egeberg DL, Alvarez L, Brenker C, Rehfeld A, et al. 2014. Direct action of endocrine disrupting chemicals on human sperm. EMBO Rep 15(7):758–765, PMID: 24820036, https://doi.org/10.15252/embr.201438869.
53. Heudorf U, Letzel S, Peters M, Angerer J. 2000. PCP in the blood plasma: current exposure of the population in Germany, based on data obtained in 1998. Int J Hyg Environ Health 203(2):135–139, PMID: 11109565, https://doi.org/10.1078/S1438-4639(04)70018-8.
54. Reigner BG, Rigod JF, Tozer TN. 1992. Disposition, bioavailability, and serum protein binding of pentachlorophenol in the B6C3F1 mouse. Pharm Res 9(8):1053–1057, PMID: 1409377, https://doi.org/10.1023/a:1015810629245.
55. Klemmer HW, Wong L, Sato MM, Reichert EL, Korsak RJ, Rashad MN. 1980. Clinical findings in workers exposed to pentachlorophenol. Arch Environ Contam Toxicol 9(6):715–725, PMID: 7469482, https://doi.org/10.1007/BF01055546.
56. Cline RE, Hill RH, Phillips DL, Needham LL. 1989. Pentachlorophenol measurements in body fluids of people in log homes and workplaces. Arch Environ Contam Toxicol 18(4):475–481, PMID: 2774665, https://doi.org/10.1007/BF01055012.
57. Reagan-Shaw S, Nihal M, Ahmad N. 2008. Dose translation from animal to human studies revisited. FASEB J 22(3):659–661, PMID: 17942826, https://doi.org/10.1096/fj.07-9574LSF.
58. Walton K, Dorne JL, Renwick AG. 2001. Uncertainty factors for chemical risk assessment: interspecies differences in the in vivo pharmacokinetics and metabolism of human CYP1A2 substrates. Food Chem Toxicol 39(7):667–680, PMID: 11397514, https://doi.org/10.1016/s0278-6915(01)00006-0.
59. Bautista DM, Jordt S-E, Nikai T, Tsuruda PR, Read AJ, Poblete J, et al. 2006. TRPA1 mediates the inflammatory actions of environmental irritants and proalgesic agents. Cell 124(6):1269–1282, PMID: 16564016, https://doi.org/10.1016/j.cell.2006.02.023.
60. McNamara CR, Mandel-Brehm J, Bautista DM, Siemens J, Deranian KL, Zhao M, et al. 2007. TRPA1 mediates formalin-induced pain. Proc Natl Acad Sci USA 104(33):13525–13530, PMID: 17686976, https://doi.org/10.1073/pnas.0705924104.
61. Liverman CS, Brown JW, Sandhir R, Klein RM, McCarson K, Berman NEJ. 2009. Oestrogen increases nociception through ERK activation in the trigeminal ganglion: evidence for a peripheral mechanism of allodynia. Cephalalgia 29(5):520–531, PMID: 19210515, https://doi.org/10.1111/j.1468-2982.2008.01755.x.
62. Thomsen L, Kruuse C, Iversen H, Olesen J. 1994. A nitric oxide donor (nitroglycerin) triggers genuine migraine attacks. Eur J Neurol 1(1):73–80, PMID: 24283432, https://doi.org/10.1111/j.1468-1331.1994.tb00053.x.
63. Al-Karagholi MA-M, Hansen JM, Guo S, Olesen J, Ashina M. 2019. Opening of ATP-sensitive potassium channels causes migraine attacks: a new target for the treatment of migraine. Brain 142(9):2644–2654, PMID: 31292608, https://doi.org/10.1093/brain/awz199.
64. Bates EA, Nikai T, Brennan KC, Fu Y-H, Charles AC, Basbaum AI, et al. 2010. Sumatriptan alleviates nitroglycerin-induced mechanical and thermal allodynia in mice. Cephalalgia 30(2):170–178, PMID: 19489890, https://doi.org/10.1111/j.1468-2982.2009.01864.x.